LEVEL

## Technical Report

538

D. C. Shaver

# Alignment of Liquid Crystals by Surface Gratings

DTIC
SELECTED
JUL 1 7 1980

C

31 October 1979

# Lincoln Laboratory

### MASSACHUSETTS INSTITUTE OF TECHNOLOGY

LEXINGTON, MASSACHUSETTS

80  7  14  023

This technical report has been reviewed and is approved for publication.

FOR THE COMMANDER

Raymond L. Loiselle, Lt. Col., USAF
Chief, ESD Lincoln Laboratory Project Office

# MASSACHUSETTS INSTITUTE OF TECHNOLOGY
## LINCOLN LABORATORY

# ALIGNMENT OF LIQUID CRYSTALS
# BY SURFACE GRATINGS

*D. C. SHAVER*

*Group 87*

TECHNICAL REPORT 538

31 OCTOBER 1979

LEXINGTON                                    MASSACHUSETTS

# ALIGNMENT OF LIQUID CRYSTALS BY SURFACE GRATINGS[*]

## ABSTRACT

Square-wave grating structures with periodicities ranging from 3200 Å to 12 µm were etched into fused quartz substrates, and the effect of such gratings on liquid crystal alignment was studied. Gratings with periodicities below 4 µm appear to be required to align typical room-temperature nematic liquid crystals. At larger periodicities a pronounced defect texture forms. The defect texture is created during nucleation and growth of the nematic phase as it cools from the isotropic phase. The defect texture is stabilized by adsorption of an oriented molecular layer on the substrate surfaces. This adsorbed layer exerts an orienting torque on the bulk liquid crystal. Experiments were performed to demonstrate the existence of such an adsorbed layer.

The tilt angle of the nematic director from the plane of quartz substrates was measured for liquid crystals used in the alignment experiments. M24 and the heptyl/butyl mixture align with the director in the substrate plane. MBBA aligns with a tilt angle of about 23 deg on fused quartz, whether or not a grating structure is present.

Surface gratings were also formed by patterning a monolayer of DMOAP. Such patterned organic monolayers, which have no appreciable surface relief, are effective at aligning liquid crystals. This represents a new approach to liquid crystal alignment.

High-quality alignment of the smectic A phase of M24 was induced by a 3200-Å-period square-wave surface-relief grating.

A novel twisted-nematic liquid crystal display which uses metal gratings for polarization of light as well as for liquid crystal alignment was fabricated.

---

# CONTENTS

v

# ACKNOWLEDGMENTS

## CHAPTER 1
## INTRODUCTION

### 1.1 BASIC PROPERTIES OF LIQUID CRYSTALS

Many organic compounds exist in phases with properties intermediate between those of conventional isotropic liquids and those of crystalline solids. In crystals, all the molecules occupy positions at well-defined sites on a three-dimensional lattice; furthermore, if the molecules are not spherically symmetric so that the "orientation" of a molecule can be specified, then the molecules are found to be oriented with respect to the lattice. In an isotropic liquid, no long-range order exists either translationally or orientationally. Between the extremes represented by crystals and isotropic liquids, matter may exist in forms, called mesophases, with intermediate degrees of molecular order. The term "liquid crystals" has been given to mesophases which retain orientational ordering but have lost translational order in one or more dimensions. In nematic liquid crystals, the centers of mass of the molecules are randomly positioned, except for very short range correlations, but the molecules tend to orient in a single direction. The large mobilities of the molecules impart the property of fluidity to the nematic phase. Figures 1(a) and (b) show two examples of nematic ordering. In both cases the centers of mass of the molecules are randomly placed, but in Fig. 1(a) the orientational order is perfect while in Fig. 1(b) a direction of orientation is statistically preferred though any single molecular orientation may depart substantially from the preferred direction. The case of Fig. 1(b) corresponds to what occurs in nature; the thermal energies of the molecules are comparable to the depth of the orientational potential well which the molecules sit in, so the molecules are not uniformly oriented, and many molecules undergo complete rotations.

Figure 1(c) illustrates another type of liquid crystalline phase, the smectic A phase. In addition to orientational order, one-dimensional translational order exists. The molecules form layers with a well-defined spacing though the centers of mass of the molecules are randomly placed in two dimensions within the layer. In fact, the layers in the smectic A phase do not have a perfect long-range order and considerable diffusion of molecules occurs between layers, but this phase is nonetheless considerably more ordered than the nematic phase.

Nematic liquid crystals undergo a first-order phase transition to an isotropic phase upon heating to the transition temperature, $T_{NI}$. Smectic A phases may transform into nematic phases upon heating or they may transform directly to the isotropic liquid phase.

A nematic or smectic A phase, in the absence of external forces, will form a large domain of statistically uniform alignment. That is, within the domain an axis can be defined which represents the average direction of alignment of the liquid crystal molecules. The liquid crystal and all its properties are invariant to rotation about this axis, and properties such as the dielectric constants are different when measured along the axis vs in a direction perpendicular to that axis. Thus, nematic and smectic A materials are uniaxial.

The intermolecular forces favor unidirectional alignment of the molecules, but the alignment can be altered by applying external forces. The alignment of the molecules in a distorted nematic can be described by means of a vector field. For each point in the liquid crystal a unit

1

(a)

NEMATIC
S = 1

$\uparrow \vec{n}$
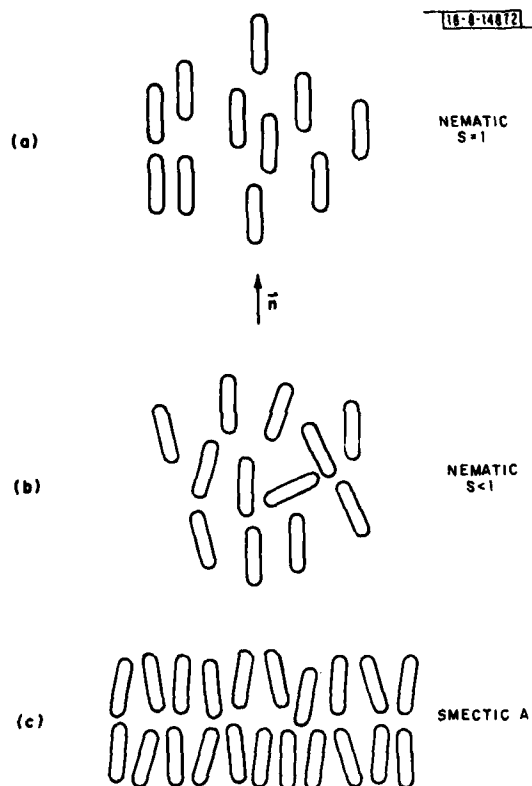
Fig. 1. Schematic representation of different liquid crystalline phases. S is the order parameter and represents the degree of orientational order.

(b)

NEMATIC
S < 1

(c)

SMECTIC A

vector $\hat{n}$, called the nematic director, points in the average direction of alignment of the molecules at that point. In nematic liquid crystals the "heads" or "tails" of the molecules do not orient in a single direction; roughly equal numbers of heads and tails point in the same direction. Thus, the liquid crystal has two-fold symmetry for rotations in a plane containing the nematic director. This means that the nematic director cannot be uniquely defined; an equivalent nematic director which points in the opposite direction exists.

## 1.2 DISTORTION OF NEMATIC LIQUID CRYSTALS BY BOUNDARIES

At the boundaries of a nematic fluid, certain nematic director orientations relative to the bounding surface may be energetically preferred. For instance, the liquid crystal MBBA[*] orients with its nematic director perpendicular to the surface of glass coated with the silane coupling agent DMOAP[†] (see also Ref. 1). On crystalline surfaces, the director may be constrained to point in a limited set of directions corresponding to crystallographic axes, as in the case of p-azoxyanisole on sodium chloride crystals.[2]

Thus, the total free energy, F, of a liquid crystal enclosed by boundaries is:

$$F = F_e + F_s \tag{1-1}$$

---

[*] MBBA is N-(p-methoxybenzilidene)-p-butylaniline.

[†] DMOAP is N,N-dimethyl-N-octadecyl-3-aminopropyltrimethoxysilyl chloride; available from Dow Corning, Midland, Michigan, as silane XZ-2230.

2

where $F_e$ is the elastic distortion energy which is nonzero if the nematic director is not unidirectionally oriented and $F_s$ is the energy contribution of the molecules at the boundary. That is,

$$F_s = \oiint_S g(x, y, z) \, dS \tag{1-2}$$

where $g(x, y, z)$ is the energy per unit area at each point on the boundary surface. $g(x, y, z)$ depends on the orientation of the nematic director with respect to the surface and on the surface material.

The equilibrium orientation of the liquid crystal is found by minimizing $F$ with respect to $\hat{n}(x, y, z)$. The surface energy contribution is particularly difficult to evaluate. The orientation of the nematic director with respect to a specific surface can be relatively easily determined experimentally in the case when there is no elastic deformation of the liquid crystal. The orientation observed is in fact the orientation which results in the minimum value for the surface energy density, $g$. Determining the energy required to deform the director orientation at the surface from its minimum energy state to some new direction is quite difficult and these energy dependences are not known.

The problem of determining surface energies can be avoided and the entire alignment energy calculation can be greatly simplified by assuming tight binding of the liquid crystal molecules at the boundary. If one assumes that the energy required to change the orientation of the nematic director at the surface is very large, then (a) the boundary conditions at the surface become fixed and (b) there is no dependence of the surface energy on the director orientation in the bulk liquid crystal. Tight binding does not mean that the nematic director at the boundary is completely specified, however. A number of orientations of equivalent energy may have to be considered if the energy minimum at the surface does not correspond to a single orientation. In the case where $\hat{n}(x, y, z)$ is completely specified at the boundaries, determining the equilibrium configuration of the liquid crystal simply involves finding $\hat{n}(x, y, z)$ so that the total elastic energy $F_e$ is minimized, where

$$F_e = \iiint_V E_d(x, y, z) \, dV \tag{1-3}$$

and

$E_d(x, y, z)$ = elastic distortion energy per unit volume

$$E_d = \frac{1}{2} [K_1 (\nabla \cdot \hat{n})^2 + K_2 (\hat{n} \cdot \nabla \times \hat{n})^2 + K_3 |\hat{n} \times \nabla \times \hat{n}|^2] \quad . \tag{1-4}$$

This equation (Ref. 3) describes the elastic distortion energy density in terms of three types of distortion, splay, twist, and bend, with elastic constants (in dynes) $K_1$, $K_2$, and $K_3$, respectively.

Now we can consider the aligning properties of surfaces. Let us assume that the nematic director is constrained to lie in the plane of a smooth surface, but that all orientations within that surface plane are of equal surface energy. An undistorted nematic fluid (i.e., unidirectional director throughout the volume) can be placed in an infinite number of orientations while satisfying the boundary condition that $\hat{n}$ lie in the substrate plane. In Fig. 2 a square-wave grating structure is shown in perspective. If an undistorted nematic layer has its director in the horizontal (x-z) plane, then the boundary conditions at the bottoms of the grooves and on the plateaus

3

are satisfied. Matching the boundary conditions on the sidewalls requires that $\hat{n}$ lie in the vertical (y-z) plane. The intersection of these two planes is the z axis which is along the groove direction. Thus, a single direction of alignment exists for which there is no elastic deformation of the liquid crystal layer and for which the surface energy is a minimum.

In fact, any structure (periodic or aperiodic) which has a surface relief which varies in the x direction but is invariant in the z direction will allow nematic alignment in the z direction with an absolute minimum in the free energy, given the tangential $\hat{n}$ boundary condition. All other alignment directions will result in some elastic free energy contribution.
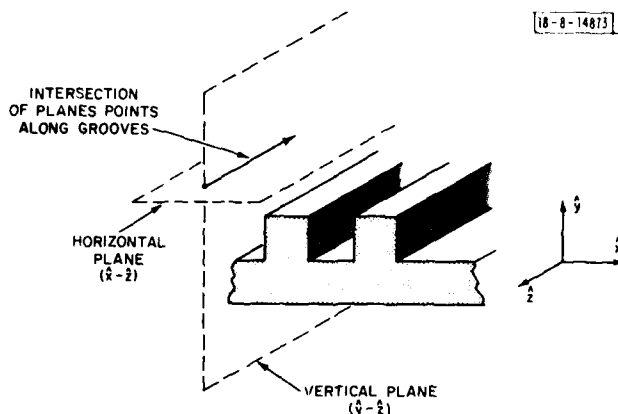


Fig. 2. A square-wave grating structure showing the boundary conditions imposed on a liquid crystal whose director is constrained to lie in the surface plane. For minimum bulk distortion, the director is constrained to lie both in the horizontal and the vertical planes, so the alignment direction is along the grooves.

## 1.3 INDUCING ALIGNMENT OF NEMATICS BY SURFACE TREATMENT

Based on the arguments presented above, one might expect that a surface with a relief structure would be capable of aligning liquid crystal layers. The liquid crystals p-azoxyanisole (PAA) and p-azoxyphenetole were aligned in 1928 by Zocher[4] using glass surfaces which were made anisotropic by unidirectional rubbing with filter paper or cotton wadding. Zocher also observed that methylene blue, a dye, formed oriented layers on rubbed surfaces if an alcohol solution of the dye was evaporated rapidly. Zocher tried unsuccessfully to produce oriented films of inorganic substances such as potassium chloride, potassium iodide, and ice on rubbed surfaces. It is significant that alignment of potassium chloride crystallites was recently achieved on square-wave grating structures by Flanders[5] at M.I.T. Lincoln Laboratory.

Since Zocher's early experiments, liquid crystals have become widely used in electronic display devices and unidirectional alignment of the director in the plane of a transparent substrate is often required. A number of techniques for producing a predetermined alignment of the director at surfaces have been investigated, and a few of these methods will be discussed briefly.

Orientation of the director perpendicular to a surface can be achieved by using silane coupling agents such as DMOAP or soaps such as CTAB (see † footnote on p. 2; also Refs. 1, 6-8). Proust et al.[7] have shown that either perpendicular (homeotropic) or parallel (often called "homogeneous") orientation of the director at the surface can be achieved by varying the surface concentration of CTAB. The direction of substrate withdrawal from the CTAB solution further determines the alignment direction in the substrate plane for the case of homogeneous alignment. In many display applications, orienting molecular layers such as lecithin or CTAB are unsatisfactory. First, the aligning properties of these organic layers may be destroyed if high substrate temperatures are attained during frit sealing of liquid crystal cells, and second, the organic layer may desorb from the substrate over time, resulting in loss of alignment.

Because of problems with the durability of organic layers, alignment methods which rely only on the surface topography and the liquid crystal-substrate molecular interactions are often preferred. Rubbing methods are still extremely popular and have been used by many experimenters to produce unidirectional alignment.[9-12] The main technological improvement in rubbing has been to use various abrasives such as fine-grain diamond paste. When abrasives are used, striations are clearly visible in scanning electron micrographs[9] or transmission electron micrographs of shadowed replicas[10-12] of the substrate surface. In contrast, rubbing of surfaces without abrasives does not produce a discernible surface topography[9] and the alignment effects are not as stable. It is possible that unidirectional rubbing without abrasives may produce striated organic deposits on the surface, rather than a pattern of grooves in the substrate. It will be shown in this report that patterned organic monolayers may have alignment properties similar to those of surface-relief structures.

Janning[13] has described a technique for producing a surface topography which is very effective in aligning nematic liquid crystals. A thin layer ($<100$ Å) of gold or SiO is evaporated onto a substrate at a very shallow angle from the substrate plane (85° from the substrate normal). The unidirectional impingement of material at these shallow angles creates an oriented surface texture, possibly a fiber texture oriented toward the evaporation source.[14] Guyon et al.[15,16] demonstrated that the nematic director will align perpendicular to the plane of incidence of the evaporated material and in the substrate plane for evaporations at 45° to 80° from the substrate normal; for angles of incidence greater than 80° the director points 20° to 30° out of the substrate plane and in the plane of incidence of the evaporant. Meyerhofer[17] and others[18] have used combinations of oblique evaporations at different angles of incidence to produce unidirectional alignment with small but nonzero tilt angles. Control of both alignment and tilt angle can be achieved using such combinations, but our understanding of these alignment methods is largely empirical.

The topography of these "obliquely evaporated" films has generally been considered responsible for their alignment properties. Obliquely evaporated SiO films on carbon membranes[19] and shadowed replicas of SiO layers[20] have been examined in the transmission electron microscope in order to correlate surface topography with alignment properties. Figure 3 of Ref. 19 reveals a "striated" texture in obliquely evaporated films. The surface topography can really only be described as a texture, since a reproducible pattern of surfaces features is not produced.

Shallow angle ion-beam etching[21,22] has been used to produce an anisotropic surface for unidirectional alignment of nematic films. Again, surface topography is presumed to be responsible for the alignment effects.

## 1.4 ALIGNMENT OF LIQUID CRYSTALS BY PLANAR FABRICATED SURFACE STRUCTURES

I have already shown that for a square-wave structure (or, more generally, fo. any "one-dimensional" surface structure) alignment of the nematic director along the grooves yields a minimum in the surface free energy and no elastic deformation energy for the case where the nematic director is required to be tangent to the surface. Berreman[10,11] and Wolff et al.[12] have performed theoretical calculations of the free energy required to misalign the director on low-amplitude, sinusoidal surface-relief structures.

Rubbing techniques may produce a high density of reasonably parallel grooves and the fact that rubbed surfaces align liquid crystals can be considered evidence that a grooved structure induces alignment to minimize elastic deformation energy. Other interpretations are possible, however, since surfaces rubbed with paper which do not reveal any grooves[9] also align liquid crystals, it is possible that rubbing of surfaces may produce some other (invisible) form of surface anisotropy which is primarily responsible for liquid crystal alignment.

If a grating pattern were exposed in a photoresist layer on a surface, and if the resulting pattern in the photoresist layer could be etched into the surface, then an anisotropic surface structure could be produced without unidirectional rubbing or scratching of the surface; the only anisotropy is in the pattern itself. Liquid crystal alignment by a grooved surface would be demonstrated simply and directly by such an experiment. Other advantages of such "planar process" structures are (a) sources of residual elastic deformation which are always present on rubbed surfaces, such as nonparallel grooves, rough sidewalls of grooves, and defects and discontinuities in the grooves can be almost completely eliminated and (b) the density, depth, and configuration of the grooves are directly controlled during processing of the surface, making it possible to do quantitative studies of surface alignment forces.

The procedure described above of exposing a pattern of lines in a resist, etc., was referred to as a "planar process." Many techniques can be considered as "planar processes" but the essential elements of the planar process as referred to in this report are (a) a well-defined pattern of surface structures is fabricated instead of a texture, (b) the actual surface structure is formed in or on the surface simultaneously and not by serial mechanical means, and (c) the process steps do not have an anisotropy which need be correlated with the groove direction, as in rubbing, scribing, or oblique evaporation.

Surprisingly, no experiments where liquid crystals were aligned by planar fabricated surface structures have been published, except for recent work performed at M.I.T. Lincoln Laboratory[5,23]. In the thesis by Flanders, the alignment of the liquid crystal MBBA by 3200-Å-period gratings was described. A number of issues related to that alignment, such as the unambiguous determination of the alignment direction and tilt angle, were undertaken as part of the present report. The subsequent chapters address the following issues:

(a) Several liquid crystals will be studied to determine their direction of orientation and tilt angle both on smooth surfaces and on surfaces containing gratings.

(b) The threshold spatial period of grooves required to align liquid crystals will be studied. The forces which induce misalignment will be discussed. Some interesting directional adsorption phenomena will be presented.

6

(c) It will be shown that a grooved relief structure is not needed to produce alignment and that liquid crystals can be aligned by planar fabricated patterned organic monolayers.

(d) A novel method of making a twisted nematic liquid crystal display using grating technology will be presented.

(e) Some ideas for future experiments made possible by planar process techniques will be presented.

# CHAPTER 2
## PROPERTIES OF ALIGNED AND MISALIGNED NEMATIC LAYERS

### 2.1 ALIGNMENT OF LIQUID CRYSTALS BY 3200-Å-PERIOD SQUARE-WAVE GRATINGS

Rubbed surfaces can provide a very high density of grooves; Berreman[11] suggests that an amplitude of 200 Å and a period of 1000 Å may be reasonable estimates of the sinusoidal modulation on such a surface. Thus, the absence of published reports on alignment by "planar fabricated" structures might indicate that surface structures with submicrometer dimensions are required and that the means for producing these structures are not widely available. Thus, for preliminary alignment experiments square-wave gratings of the minimum periodicity (3200 Å) which could be reproducibly fabricated over a reasonable (at least 1 $cm^2$) area were used.

Square-wave gratings of 3200-Å period were fabricated over a 1.25- × 1.25-cm area on two fused quartz substrates. The grooves were approximately 200 Å deep. Appendix A describes the methods used to fabricate the gratings. The two substrates were assembled into a sandwich with the surfaces containing the gratings facing each other and with 50-μm-thick Teflon spacers separating them. Figure 3 shows the assembled sandwich. Light is strongly diffracted from the gratings into beams which propagate in directions orthogonal to the groove direction. Thus, the grooves on the two substrates can be made parallel by rotating one substrate with respect
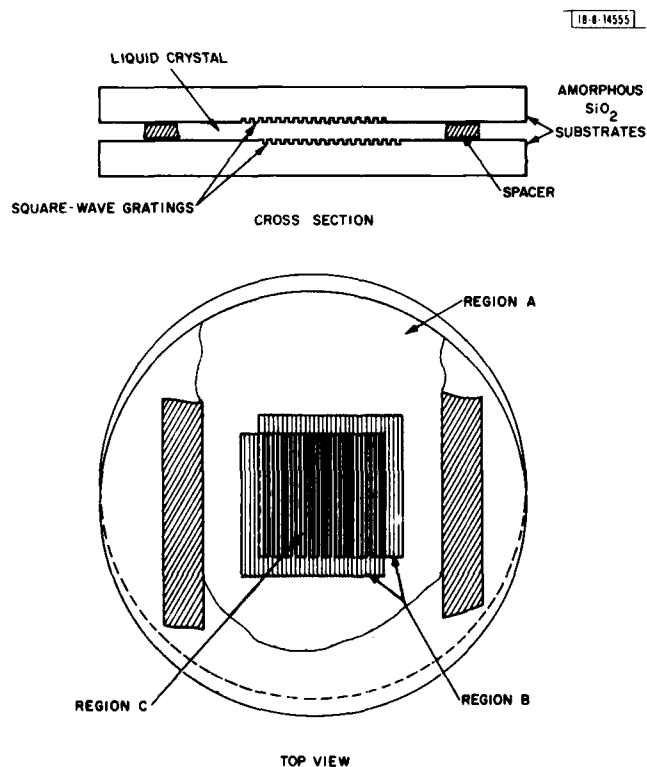


Fig. 3. "Sandwich assembly" used to test liquid crystal alignment properties of surface gratings.

to the other until the diffracted beams from the two gratings propagate in the same direction. After the substrates were aligned, the sandwich was heated and droplets of liquid crystal were placed on the lower substrate in contact with the edge of the upper substrate. The liquid crystal was sucked into the gap between the substrates by capillary action. The liquid crystal was always kept in the isotropic phase while it flowed into the sandwich; after the flow stopped, the liquid crystal was cooled to the nematic phase.

Appendix B describes in detail the different techniques used to examine the orientation of the nematic director of liquid crystal layers, including the advantages and disadvantages of the methods. The reader is referred to this appendix for details of the orthoscopic and conoscopic viewing methods.

Figure 3 shows that the liquid crystal layer is confined between two smooth surfaces in some areas of the sandwich (region A), between two gratings in other areas (region C), and also between one smooth surface and one surface with a grating (region B). Figure 4 shows a nematic layer of the heptyl/butyl mixture (see Appendix C for properties) viewed orthoscopically between crossed polarizers. The sandwich contains 3200-Å-period gratings as described above, and one polarizer is oriented along the groove direction. Figure 4 shows the boundary between a region where the liquid crystal is confined between two gratings (region C) and a region where it is in contact
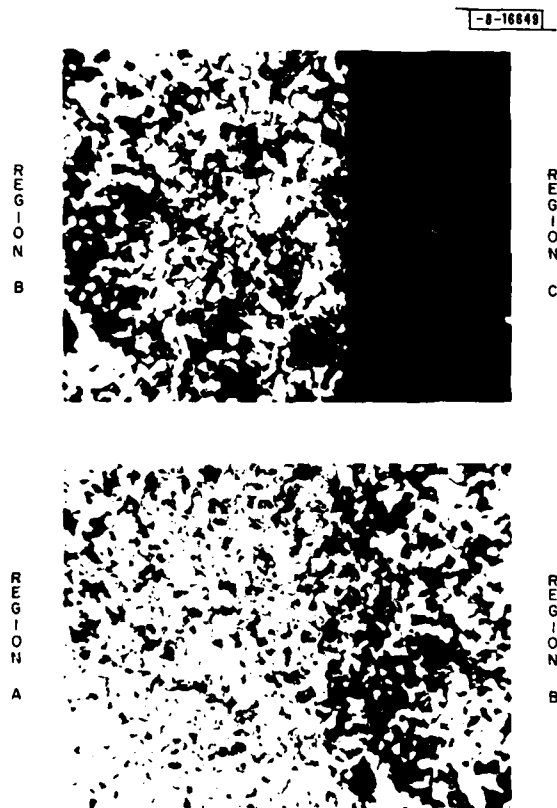


Fig. 4. Alignment of the heptyl/butyl mixture by 3200-Å-period gratings. Regions correspond to labeled regions in Fig. 3. From top to bottom of each photo is 1.2 mm.

with a smooth surface and a grating (region B). Region C is uniformly black indicating unidirectional alignment of the nematic director. Region B is not black, and many lines and discontinuities are visible, indicating highly disordered alignment. Figure 4 shows what happens at the boundary between region A and region B; region A is brighter than region B, which indicates a further loss of alignment. In region B the liquid crystal is probably well aligned on the surface with the grating but forms small "randomly" aligned patches on the smooth surface. The liquid crystal between the surfaces must then undergo a twist, but the cell thickness is great enough that the distortion energy is small and the molecules on the smooth surface are obviously held securely enough that the small torques favoring alignment are ineffective.

Figure 5(a) shows the border between region A (top of photo) and region C (bottom) using the same gratings, but with MBBA as the liquid crystal. Region B (middle) is predominantly aligned by the grating in contrast to region B of Fig. 4; either the surface forces which create twisted regions are weaker or MBBA is stiffer than the heptyl/butyl mixture, increasing the torque. This will be discussed later. Figure 5(b) shows the MBBA nematic film in region A. The film is not well aligned, and the pattern is a "Schlieren texture," which is commonly observed in nematic films.[24-27]



NO GRATINGS

TWO GRATINGS

(a)

Fig. 5. Alignment of MBBA by 3200-Å-period gratings. Top to bottom of each photo is 0.5 mm.

NO GRATINGS

(b)

11
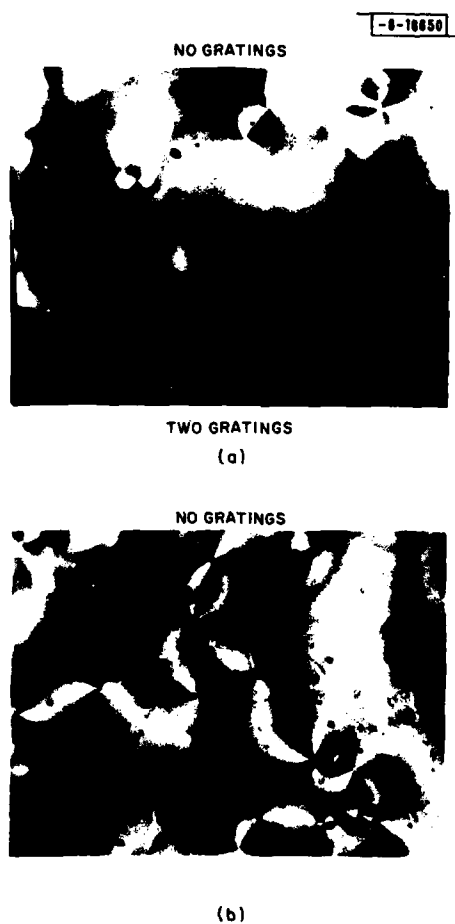
The gratings produce excellent alignment of the nematic director. A null in the transmission (black field) during orthoscopic observation between crossed polarizers occurs when the grooves are aligned within approximately 1° of the polarizer direction. Sharp nulls occur every 90° as the sample is rotated; we can only deduce that the nematic director projection on the substrate plane is oriented along or perpendicular to the groove direction, ±1°.

Conoscopic examination of the liquid crystal layer gives further information about the alignment of the director. Figures 6(a) and (b) show the conoscopic patterns for MBBA and the heptyl/butyl mixture, respectively. In both cases the liquid crystal is aligned between 3200-$\overset{\circ}{A}$-period gratings, the grooves are at an angle of 45° from the polarizer direction, the nematic layer is 50 μm thick, and monochromatic illumination from a sodium lamp (5890 $\overset{\circ}{A}$) is used. The objective lens has a numerical aperture of 0.65 for all conoscopic photos in this report. From Fig. 6(a) we can see that the nematic director for MBBA does not lie in the plane of the surface, but tilts away from the plane. In contrast, the heptyl/butyl mixture nematic director lies in the plane of the substrate, as evidenced by Fig. 6(b).



(a)
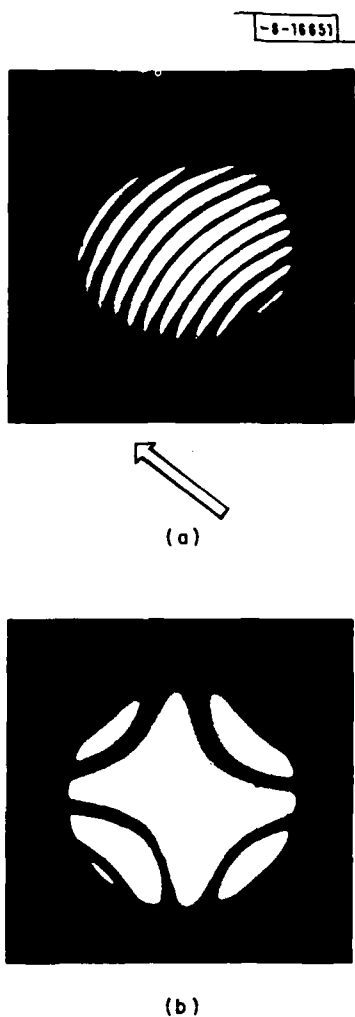
Fig. 6. Conoscopic photos showing tilt angle of (a) MBBA and (b) heptyl/butyl mixture on fused quartz substrates, with alignment by 3200-$\overset{\circ}{A}$-period gratings.



(b)

12

Further examination of Fig. 6 reveals that the pattern of Fig. 6(a) is symmetric about a single axis, whereas the pattern of Fig. 6(b) has two axes of symmetry. In Fig. 6(a) the axis of symmetry must correspond to the projection of the nematic director on the substrate plane, since the conoscopic pattern is always symmetric about the director. For liquid crystals, like MBBA, whose nematic directors tilt away from the substrate plane, the conoscopic pattern reveals unambiguously the direction of the nematic director projection. The grooves did run in the same direction as the axis of symmetry of Fig. 6(a). Combining this result with the result of orthoscopic examination, we can say that for MBBA the nematic director projection aligns along the grooves within 1°, and that the director tilts away from the substrate plane.

Though the conoscopic pattern of Fig. 6(b) shows that the heptyl/butyl director lies in the substrate plane, it still does not permit discrimination between alignment along the grooves and perpendicular to them, as discussed in Appendix B. By using a dye which aligns with the nematic director (see Appendix B) it was shown that the nematic director does lie along the groove direction for the heptyl/butyl mixture. Furthermore, the dye technique was applied to MBBA and is in agreement with the conoscopic interpretation; the director projection lies along the groove direction.

## 2.2 TILT ANGLE OF LIQUID CRYSTALS ON GROOVED AND UNGROOVED SUBSTRATES

Conoscopic evidence indicates that the heptyl/butyl mixture nematic director lies in the plane of a fused quartz substrate while MBBA forms a tilt angle with the surface. M24 was another liquid crystal used for alignment experiments. It was not possible to check the alignment of the liquid crystal M24 conoscopically because the sample was maintained inside a temperature-controlled chamber whose thickness prevented us from using high numerical aperture objectives. Examination of Schlieren textures found in nematic layers of M24 revealed no reverse-tilt walls attached to disclinations of strength 1/2. Following the discussion in Appendix B, this is strong evidence that the nematic director lies in the plane of the fused quartz substrate.

The result that the nematic director of MBBA tilts away from the substrate plane seemed quite surprising. There is controversy about whether MBBA orients parallel or perpendicular to clean glass, but no reports of tilted alignment have appeared. In fact, special techniques, such as the bonding of short chain alcohols to quartz[22] or oblique evaporation methods,[18] have been developed specifically to permit alignment of liquid crystals with controlled tilt angles.

Several questions arose about the director tilt of MBBA on fused quartz:

(a) What is the tilt angle?

(b) Is the tilt induced by the presence of the grating or is it the same on smooth fused quartz?

(c) Is the tilt caused by organic contaminants on the surface?

(d) Is the tilt a consistent behavior on quartz?

(e) Is contamination of the liquid crystal responsible for the tilt?

(f) Is it possible that fused quartz substrates may behave quite differently from other glasses, at least with respect to tilt properties of MBBA?

The tilt angle of MBBA on fused quartz was estimated in three experiments using two different measurement methods. In one experiment, substrates with 3200-Å-period gratings were used, and the effective birefringence of the MBBA was measured using the "wedge technique" described in Appendix B, Sec. B.2. The birefringence measured for rays normally incident on the nematic layer was 0.185, with an error bound of less than ≈10 percent. This corresponds to a nominal tilt of 23° between the director and the substrate plane. The room-temperature values for the refractive indices of MBBA at 5890 Å given in Appendix C were used for the tilt angle calculation. It was also the case that the fringes observed using the "wedge technique" continued in a straight line across the boundary between region C (two gratings) and region A (no gratings) of Fig. 3. This indicates that the nematic director has the same tilt angle on smooth fused quartz as in the grating area. The gratings do not appear to be responsible for the tilting of MBBA.



Fig. 7. Conoscopic photo showing the tilt angle of MBBA when confined between 12-μm-period gratings. A reasonably uniformly aligned patch was selected for conoscopy.

Figures 6(a) and 7 show conoscopic patterns of MBBA layers confined between 3200-Å and 12-μm-period gratings, respectively. In both cases, 12 black fringes are visible. As discussed in Appendix B, Sec. B.3, these fringe patterns are consistent with a tilt angle of 23°. As is the case for the "wedge technique," the refractive indices must be known to perform the tilt calculation, and the same values from Appendix C were used. Conoscopic patterns also indicated that the director was tilted outside the grating area, but the patterns were of poor quality, making quantitative estimates from, or photography of, the patterns quite difficult.

Considerable controversy exists about the tilt angle of MBBA on clean glass. Creagh and Kmetz[9] studied the alignment of MBBA on tin-oxide-coated glass. They showed that MBBA

14

aligns perpendicular to carefully cleaned tin oxide, but it aligns parallel to the surface if a thin carbon film is deposited. Lecithin-coated tin oxide causes perpendicular alignment of MBBA. Creagh and Kmetz also state that MBBA aligns perpendicular to clean glass, though all their experiments appear to be with tin-oxide-coated glass. They propose that the difference between the critical surface energy of the substrate and the surface tension of the liquid crystal deter- mines whether parallel or perpendicular alignment of the director occurs; the possibility of tilted alignment seems to be implicitly forbidden. The fact that clean glass has a high surface energy and would be expected to cause parallel alignment of the director is explained away by assuming that adsorption of water on the glass lowers the critical surface energy. Haller[28] gives numerous examples which show that the difference between the surface energy of the sub- strate and the surface tension of the liquid crystal is not, in fact, a useful predictor of the tilt angle of the director. The theory provided by Creagh and Kmetz seems to have little validity, but their work does point out that surface cleanliness and surface hydration may be determinants of the tilt angle formed by the director. Furthermore, their work indicates that MBBA aligns perpendicular to clean glass.

A number of authors have stated that MBBA aligns with its director in the plane of a "clean glass" substrate (Refs. 7, 8, 11, 12, 21). Most authors do not describe how they determined that the director was in the substrate plane, and the tilt angle may not actually have been measured. Also, considerable variation in the "glass" substrates may exist. For instance, Little et al.[21] used sputtered $SiO_2$ coatings, Berreman[11] used fused quartz, and many authors do not specify the type of glass used. There is evidence that the type of glass surface used may influence the liquid crystal tilt angle. Goodman[29] indicates that migration of alkali-ions to the substrate sur- face during heating of soda lime glass affects the alignment properties of the surface.

Several experiments were performed to see if substrate cleanliness or surface hydration affected the tilt angle of MBBA. Table I shows some of the different cleaning processes used. Process A was the standard cleaning procedure. Fused quartz substrates cleaned in this man- ner were evenly wetted by deionized water, and during blow drying of the substrates with nitro- gen, colored fringes were visible as the wetted region shrank. This generally indicates that the surface is very clean (<1 monolayer of hydrophobic organic contaminants).

Using the standard cleaning procedure, tilted alignment of MBBA on fused quartz was con- sistently obtained. The addition of a detergent cleaning step (process B) or of a UV/ozone clean- ing step (process C) did not affect the results. Tilted alignment of MBBA was obtained. UV/ ozone cleaning[30] is effective in removing traces of most organic contaminants including evapo- rated carbon films. Substrates which were UV/ozone cleaned were placed a few millimeters from an R-52 Mineralight* in air for periods of 10 min. or more. The lamp generates ozone and also exposes the substrates to short wavelength UV.

Even the UV/ozone cleaning may not guarantee that substrates will be free from organic contaminants, though it effectively removes such contaminants. Vig[30] has shown that exposure of clean substrates to room air for about 15 min. results in the appearance of a carbon peak in Auger electron spectra of the surface; wetting properties, as determined by a fog test, also deteriorate over that time interval. Even though UV/ozone cleaned substrates were used im- mediately after cleaning, the time required to assemble the liquid crystal sandwich is on the order of 15 min., and it is possible that a contaminating layer may form.

---

* R-52 Mineralight Lamp, Ultraviolet Products, Inc., San Gabriel, California.

| Cleaning Steps Performed | A Standard | B Liquinox | C UV/Ozone | D Bakeout |
|---|---|---|---|---|
| **TABLE I** | | | | |
| **DIFFERENT CLEANING PROCESSES USED FOR FUSED QUARTZ** | | | | |
| Soak, 10 min. trichloroethylene | Yes | Yes | Yes | Yes |
| Soak, 10 min. acetone | Yes | Yes | Yes | Yes |
| Rinse, methanol | No | Yes | No | No |
| Rinse, running deionized water | No | Yes | No | No |
| Blow dry, nitrogen | Yes | Yes | Yes | Yes |
| Ultrasonic clean 1% Liquinox in warm deionized water | No | Yes | No | No |
| Rinse, running deionized water | No | Yes | No | No |
| Soak, 5 to 10 min. concentrated sulfuric acid, 25°C | Yes | Yes | Yes | Yes |
| Rinse, running deionized water | Yes | Yes | Yes | Yes |
| Hot deionized water cascade rinse | Yes | Yes | Yes | Yes |
| UV/ozone clean | No | No | Yes | No |
| Dehydration bake 1 hr, 120°C | No | No | No | Yes |

Process D was used to see if the tilt angle could be affected by a change in surface hydration. Fused quartz substrates were baked at 120°C for 1 hr in a vacuum oven while dry nitrogen was flowed continuously through the oven. The substrates were assembled into a sandwich and the gap was filled with MBBA immediately after removal from the oven. According to the data provided by Creagh and Kmetz on surface hydration, this process should have reduced the adsorbed water layer substantially. Again, the director of MBBA tilted away from the substrate plane.

Reactive-ion etching (RIE) in $CHF_3$ was another step likely to produce surface contamination, and this method has not been used by any other workers in the liquid crystal field. Chromium masks become difficult to remove after RIE, and problems with polymer deposition on the substrate or on the chamber walls have been observed. RIE is not the cause of the tilted alignment of MBBA, however. Freshly cleaned quartz substrates which have never been reactive-ion etched also produce tilted alignment of MBBA.

In summary, it appears that the nematic director of MBBA consistently forms a tilt angle with our quartz substrates. The nominal tilt angle is 23°. This tilt is independent of the variations in the cleaning process which have been tested. Cleaning in concentrated sulfuric acid is extremely important for obtaining clean surfaces and produces the most dramatic improvement in the wetting properties of the glass of all the cleaning steps. Creagh and Kmetz[9] have shown that tin oxide cleaned in a sulfuric/nitric acid mixture is free of organic contamination.

There is no particular reason why tilted alignment of the director could not be the preferred orientation for MBBA on fused quartz. In fact, Bouchiat et al.[31] have determined from light reflectivity measurements that MBBA aligns at an angle of approximately 20° from the surface normal at an air/MBBA boundary. This gives further evidence that MBBA is not constrained to lie parallel or perpendicular to plane surfaces and that MBBA molecules may have a built-in asymmetry which favors tilted alignment of the director at certain surfaces. The fact that the angle observed by Bouchiat is roughly the complement of the tilt angle of MBBA on fused quartz may be significant.

Figure B-4 shows five different conoscopic patterns obtained from a single layer of MBBA sandwiched between two pieces of Corning 0211 glass. As can be seen, a wide range of tilt angles is observed. The substrates were cleaned using the same cleaning process which produces consistent tilted alignment on fused quartz. The 0211 glass substrates are harder to clean than quartz and often require exposure to an oxygen plasma to insure good water wetting, which may not be obtained using the standard cleaning process. The important point is that fused quartz substrates produce highly reproducible results, in contrast to the 0211 glass. Furthermore, the wide range of tilt angles obtained with a single liquid crystal layer makes it clear that variations in purity of different liquid crystal samples are probably not the prime factor in causing tilt angle variations.

Finally, it is noteworthy that MBBA can be aligned reliably either parallel or perpendicular to a fused quartz substrate. By coating quartz with DMOAP as described in Appendix A, excellent homeotropic alignment of MBBA (and the heptyl/butyl mixture) is obtained. Exposure of the DMOAP-coated quartz to the UV/ozone cleaning process for 5 min. alters the surface layer, and MBBA will now align parallel to the surface. Furthermore, the UV/ozone exposed area is not "clean" quartz; the water wetting of the surface is noticeably poorer than for clean, new fused quartz.

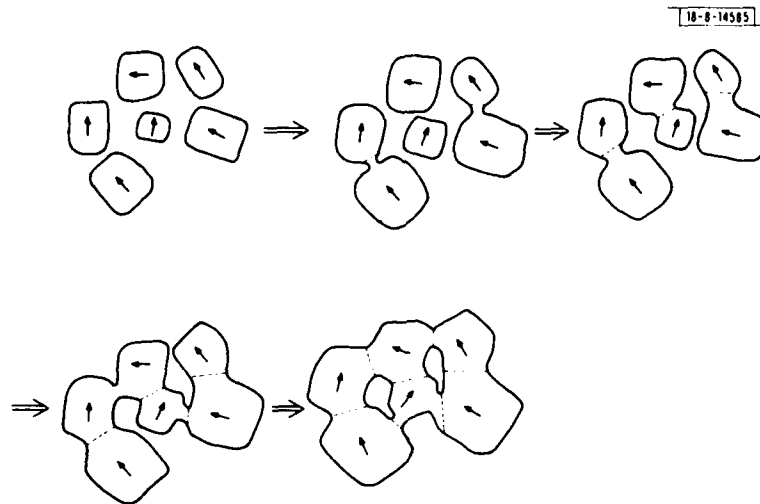18-8-14585

Fig. 8. Solid crystal thin film growth. Photo shows a case where crystallites grow but do not reorient when they contact each other. The result is a poly-crystalline film.
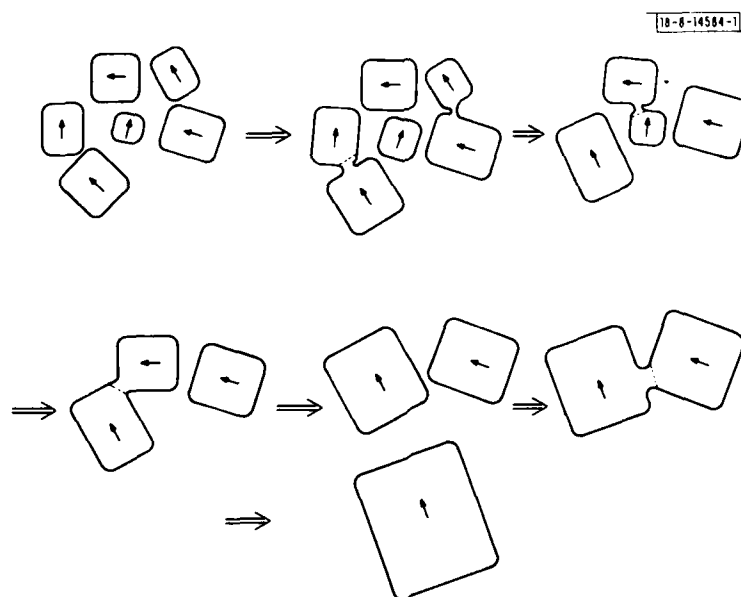


18-8-14584-1

Fig. 9. Solid crystal thin film growth. Crystallites with different orientations of their lattices reorient when they contact each other during growth. A larger and larger single crystal grain grows.

Experiments have shown that UV exposure, without ozone contact, is sufficient for altering the alignment properties of DMOAP layers as described above. It might be possible to expose patterns using UV or X-ray radiation or an electron beam in a DMOAP layer. The exposure affects the tilt angle imposed by the layer on a liquid crystal, and the patterned surface could be used to align liquid crystals. Such patterned monolayers represent a new approach to liquid crystal alignment.

## 2.3 NEMATIC LAYERS – GROWTH SCENARIO FOR SCHLIEREN TEXTURES

If a nematic liquid crystal is confined between surfaces which are "smooth" (that is, they do not have any strong anisotropy) and if the liquid crystal does not adopt the homeotropic orientation, then the nematic layer will not generally have a uniform director orientation. Nematic thin films are formed by cooling from an isotropic liquid phase. If the cooling rate is rapid, a great many "nematic nuclei," or small nematic domains, may form simultaneously at different points in the otherwise isotropic liquid crystal layer. The nematic director in these nuclei need not have any preferred orientation in the substrate plane since no surface anisotropy exists.

Consider the case of inorganic crystalline thin film growth illustrated by Figs. 8 and 9 (Ref. 5). Many small crystallites nucleate, and the orientation of the crystallites is random. As the crystallites grow and contact each other, reorientation of the crystal lattice takes place. In Fig. 8, the mobility of the deposited material is limited, and if two sufficiently large crystallites come into contact they will be unable to reorient into a single crystal. Grain boundaries will form, and a polycrystalline network results. In Fig. 9 the mobility is quite large and crystallites keep recrystallizing into larger and larger single crystal grains.

Nematic liquid crystal film "growth" after cooling from the isotropic phase proceeds along similar lines, but the characteristics of the individual "nuclei" are very different. In a solid crystal the energy required to deform the lattice is extremely large (crystals are very stiff) and each crystallite has a nearly undistorted latttice, and a single "orientation." The surface shape of the crystallite or the orientation of its entire lattice may be altered to minimize the free energy associated with the boundaries of the crystallite. For solid crystals it is energetically favorable for a crystallite to present high-energy surface planes at its boundaries rather than to deform its lattice to minimize the surface free energy. For liquid crystals the situation is reversed. The energy required to force the director to lie parallel to a surface for which its minimum free-energy orientation is homeotropic alignment is generally large compared to the energy required to deform the bulk to match the boundary conditions. This so-called "tight binding" approximation was introduced in Chap. 1. As a result, nematic nuclei will not necessarily have a single director orientation throughout their bulk. Speaking loosely, nematic nuclei need not be "single crystals" in contrast to solid crystal nuclei.

The nematic director of liquid crystals has a preferred orientation at the nematic-isotropic liquid boundary. For instance, MBBA aligns with the nematic director in the plane of the nematic-isotropic interface;[32] all orientations within that plane are equivalent in energy and free rotation of the director in the plane is possible. Meyer[33] has studied the director orientation in nematic droplets of ethyl p-(p-methoxybenzilidene amino) cinnamate. For this liquid crystal the director orients perpendicular to the nematic-air interface and parallel to the plane of the nematic-isotropic interface. Figure 10 is a cross section of one of Meyer's droplets sitting on a glass slide. The slide was warmed so that a nematic "cap" sits on a layer of isotropic liquid crystal. The director terminates normal to the air-nematic interface at all points;

19
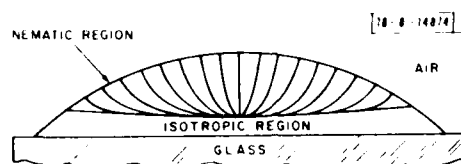
Fig. 10. Photo illustrating experiment by R. B. Meyer (Ref. 33). The glass slide is heated, causing a thin isotropic region to form under a nematic "cap." The boundary conditions cause a disclination to form in the nematic-isotropic boundary plane. Lines in nematic show the nematic director orientation.
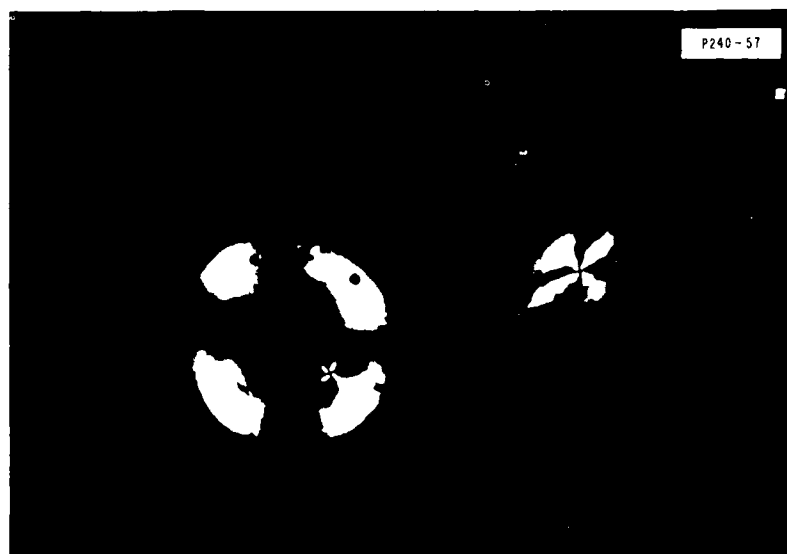


Fig. 11. Two nematic droplets of the heptyl/butyl mixture sitting on a room-temperature glass substrate. Note the disclinations resulting from the boundary conditions imposed on the director at the edges of the droplet.

in the nematic-isotropic plane which forms the base of the "cap," the director undergoes a 360° azimuthal rotation. The structure of this droplet was confirmed optically by Meyer. The boundaries of the droplet clearly determine its internal structure. Instead of unidirectional director alignment within the droplet, the topology of the boundary dictates that one point disclination with a 360° director rotation (strength = 1) will form.

Figure 11 shows two nematic droplets of the heptyl/butyl mixture sitting on a piece of clean Corning 0211 glass at room temperature. Unlike Meyer's droplets, these droplets are fully nematic. Each droplet has a single black point from which four black brushes radiate. Since the droplet is viewed orthoscopically between crossed polarizers, a black region corresponds to an area where the director projection is either parallel or perpendicular to the polarizer. Thus, a point with four black brushes indicates that the nematic director projection on the substrate plane undergoes a 360° rotation. A point with two black brushes would indicate a 180° director rotation about the point, or a so-called strength 1/2 disclination. The points from which the brushes radiate are called disclinations. Since the nematic director has two-fold symmetry, rotations of the director about a point must be multiples of 180°. In practice, disclinations of strength 1 or 1/2 are observed. The apparent "point" center of a disclination may correspond either to a point disclination on the substrate surface or to the end-on projection of a line disclination which attaches to the top and bottom substrates of the liquid crystal sandwich.

Figure 12 is a schematic representation of the arrangement of the director at disclinations. The figure shows that different signs can be defined for disclinations of equal strength. The sign of the disclination can be distinguished optically by observing the rotation of the black "brushes"
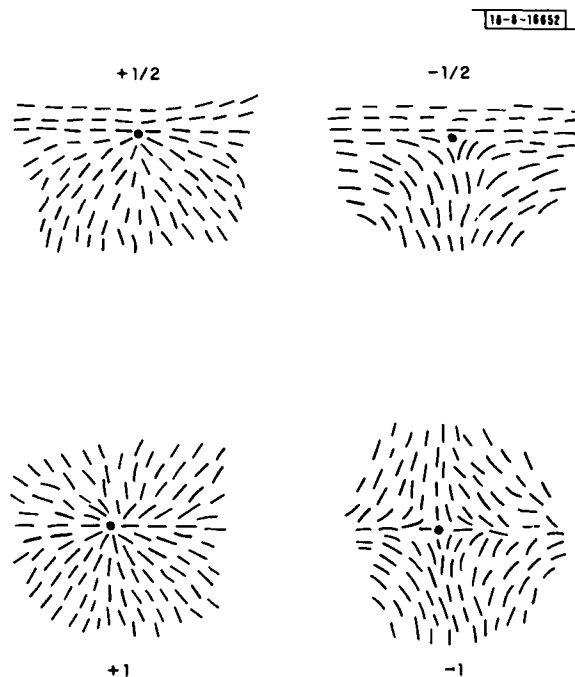


Fig. 12. Sketch showing the orientation of the director field at disclinations of different strengths and polarities.
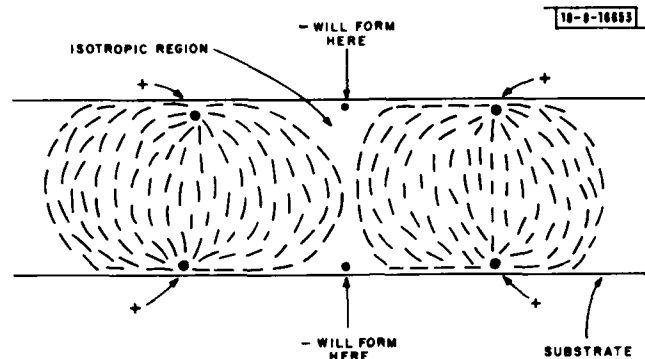
Fig. 13. Sketch showing two nematic droplets each containing two point disclinations of strength (+1). The droplets are about to combine; note that two disclinations of strength (−1) will form when the droplets touch, keeping the total strength of the disclinations in the new droplet the same.



Fig. 14. The boundary between regions of reverse tilt. (a) Possible director field if the nematic director is nearly homeotropic at the substrates and (b) if the director lies nearly parallel to the substrates.

22

as the nematic layer is rotated between crossed polarizers. For disclinations with positive sign the brushes do not rotate in the vicinity of the disclination as the microscope stage is rotated, whereas for disclinations of negative sign the brushes undergo two complete rotations for each rotation of the stage.

Now, we can speculate on the growth scenario for a nematic thin film formed by cooling an isotropic liquid. Small nematic domains form, and they will most likely form in contact with the substrate since the liquid layer is always cooled from the outside inward. As each domain forms, it will contain a disclination or disclinations; the sum of the strengths of all the disclinations in a drop is a topological property of the drop. The disclinations must form to satisfy the boundary conditions around the droplet. For instance, a droplet whose director was constrained to lie parallel to the boundary surface at all points might form with two surface disclinations of strength +1. Since the sum of the disclination strengths is a topological property of the droplet, it cannot change if the drop is stretched or otherwise distorted. Similarly, if two droplets combine to form a single drop, new disclinations must form to keep the sum of the strengths constant. This situation is sketched in Fig. 13.

There are several significant features of liquid crystal film growth that distinguish it from solid crystalline film growth. First, it should be noted that liquid crystal film growth corresponds more closely to the "high mobility" situation shown in Fig. 9 than to the "low mobility" situation of Fig. 8. "Grain boundaries" do not form in liquid crystals. Since the bulk can deform easily, discontinuities in the director orientation are energetically highly unfavorable, and are always smoothed out. Second, nematic domains are "born" with defects. A Schlieren texture arises not because of "grain" boundaries which form during the coalescence of the nuclei but because the original nuclei have a nonuniform director orientation due to the presence of disclinations.

Disclinations of opposite sign attract each other. Disclinations of equal strength but opposite sign will annihilate each other, while disclinations which are not of equal strength recombine to form a new disclination whose strength is the sum of the strengths of the original two disclinations. Even though a great number of disclinations form during the nucleation and coalescence of nematic domains, most disclinations are annihilated by others of opposite sign. Unidirectional orientation of the nematic director is the lowest free-energy state for a nematic thin film confined between two smooth surfaces. Figures 4 and 5 show that this state is not attained in practice. There is a tendency for the texture which forms during growth to stabilize and to persist for extended periods of time. The origin of the forces which prevent equilibration will be discussed in the next chapter.

Finally, it should be mentioned that certain defects may exist in nematic layers which are very well aligned. The nematic director of MBBA forms a tilt with fused quartz su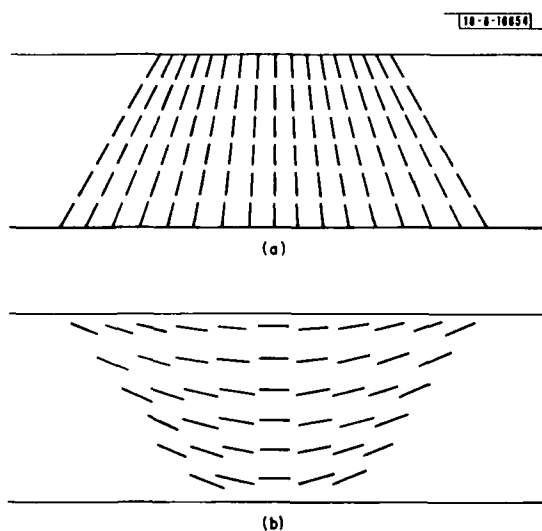bstrates, and even if the nematic director projection is aligned along the direction of grooves in the substrate, two equal energy states of opposite tilt can exist. Figure 14 shows such regions of equivalent alignment and equal but opposite tilt schematically. In Fig. 14(a) the director is nearly homeotropic, and we might expect the director to pass through the homeotropic orientation in the transition between the two regions, as shown. In Fig. 14(b), the director is nearly parallel to the substrate plane, and the transition may occur with the director becoming parallel to the substrate plane. In this case, the transition region will have increased birefringence whereas in the case of Fig. 14(a) the birefringence will decrease to zero as the tilt reverses.

23
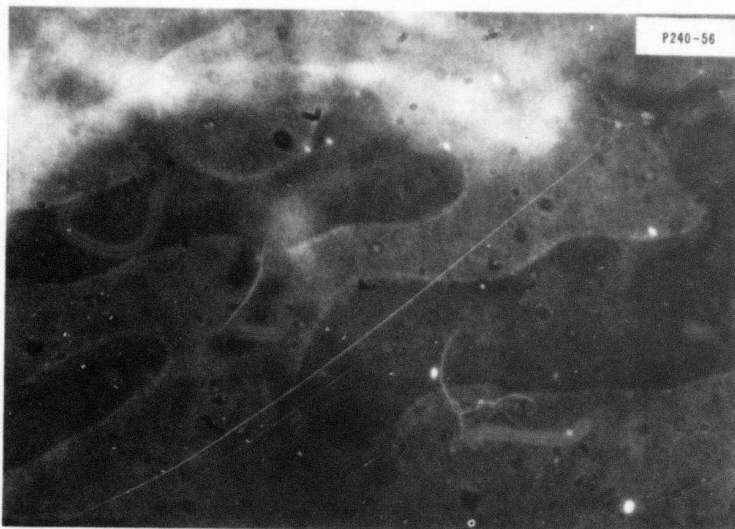
Fig. 15.  Photo showing boundaries between reverse-tilt regions in MBBA.
Top to bottom of photo is 0.5 mm.

Figure 15 shows a layer of MBBA aligned between 3200-$\overset{\circ}{A}$-period gratings formed in fused quartz.  The layer is viewed orthoscopically between crossed polarizers, and the director projection is aligned with the direction of the incident polarization.  This layer appeared uniformly black with normally incident, collimated white light.  In Fig. 15 the light source has been adjusted so the light is not normally incident.  Regions of reverse tilt are contrasted.  Examination of thin MBBA layers with white light reveals birefringence colors, and the transition region between areas of reversed tilt shows increased birefringence.  Thus, the case of Fig. 14(b) seems to represent the reverse-tilt boundaries seen with MBBA on fused quartz.  It should be noted that tilt reversal can be accomplished by other deformations than those shown in Fig. 14, and that those involving twist tend to be energetically favored.

Regions of reverse tilt are energetically equivalent and would be expected to form during the growth of nematic films.  The boundaries separating regions of reverse tilt are more similar to the grain boundaries of solid crystalline films than are the Schlieren texture disclinations. These boundaries do not represent discontinuities, as shown in Fig. 14.  The width of the transition region does provide a measure of the force exerted by the substrate which determines the lowest free-energy tilt angle of the liquid crystal.

# CHAPTER 3
## EFFECT OF SQUARE-WAVE GRATING PERIODICITY
## ON LIQUID CRYSTAL ALIGNMENT

### 3.1 MAXIMUM PERIODICITY SQUARE-WAVE GRATING REQUIRED FOR ALIGNMENT OF NEMATICS

Experiments were performed to determine the maximum period of a square-wave grating which will produce alignment of nematic liquid crystals. All gratings were etched to a depth of about 200 $\overset{\circ}{\text{A}}$. All substrates were fused quartz, but two substrates were overcoated with a 4200-$\overset{\circ}{\text{A}}$-thick layer of chemically vapor deposited (CVD) oxide ($SiO_2$). Table II summarizes the outcome of the experiments. Figures 16 to 20 show the alignment quality obtained with different periodicities and different liquid crystals.

The 3.8-$\mu$m-period grating appears to have the maximum periodicity capable of producing good alignment of MBBA and the heptyl/butyl mixture. The results with 12-$\mu$m-periodicity gratings etched into fused quartz revealed two types of misalignment of the director: (a) a Schlieren texture defect structure is visible and (b) the direction of alignment of the director in areas which are reasonably uniformly oriented is consistently misaligned with the groove direction by about 20°.

The 20° misalignment between the director and the groove direction is probably due to the presence of nearly parallel scratches resulting from the polishing of the substrate. Experiments showed that this misalignment is identical for MBBA and the heptyl/butyl mixture; thus, the similar tilt angle that MBBA forms with the substrate is probably not correlated with the angular misalignment observed here. Another experiment showed that the misalignment did not depend on the direction from which the liquid crystal was flowed into the sandwich.

| TABLE II | | | | |
|---|---|---|---|---|
| ALIGNMENT QUALITY OF LIQUID CRYSTAL LAYERS 50 $\mu$m THICK WITH GRATINGS OF VARYING PERIODICITIES | | | | |
| Grating Period ($\mu$m) | MBBA | Heptyl/Butyl | Nematic M24 | Smectic M24 |
| 0.32 | Excellent | Excellent | Excellent | Excellent |
| 1 | Good | N.A. | N.A. | N.A. |
| 3.8 | Good | Fair | N.A. | N.A. |
| 12 | Poor; consistently misaligned | Poor; consistently misaligned | N.A. | N.A. |
| 12 (in CVD layer) | Weakly aligned | N.A. | Weakly aligned | Terrible; focal conics |
| N.A. — experiment not performed. | | | | |
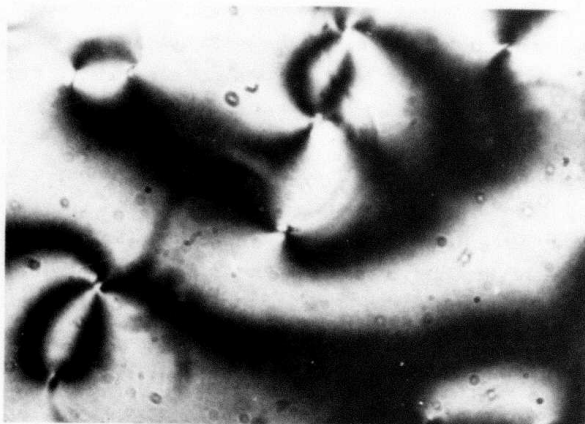
(a)

(b)

Fig. 16. Alignment of MBBA. (a) Between smooth surfaces of fused quartz substrates and (b) when confined between two 12-μm-period gratings on the surfaces.
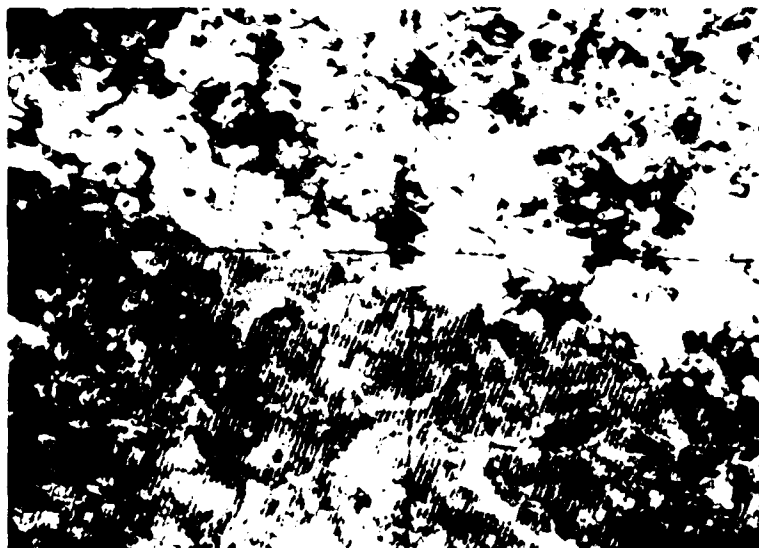
Fig. 17. Alignment of the heptyl/butyl mixture. Top right of photo shows alignment between "smooth" quartz surfaces. Bottom left of photo shows alignment between the same 12-μm-period gratings used for Fig. 16. For maximum contrast (shown) between the two regions, the grating direction was misaligned with the polarizer/analyzer directions (shown by the cross hair).

27

- 8 - 16656

(a)
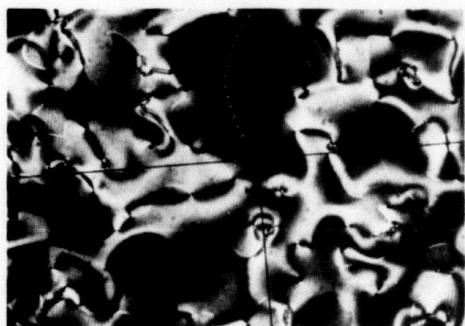
(b)

Fig. 18.  Two photos showing alignment of MBBA between 12-μm-period gratings. The gratings were formed in a CVD oxide layer deposited on the fused quartz.



- 8 - 16657
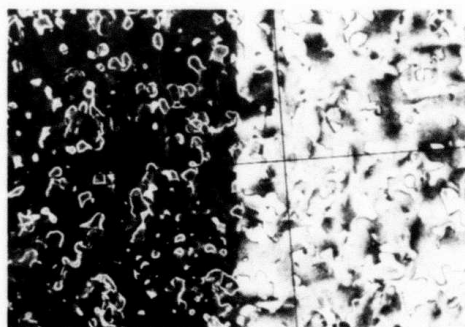
(a)
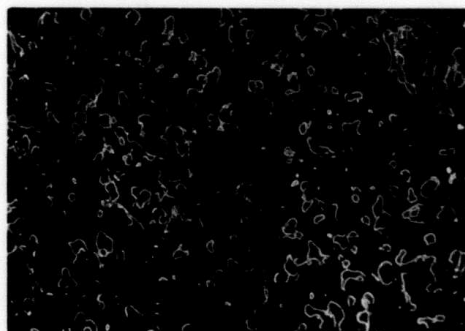
(b)

Fig. 19.  Alignment of the heptyl/butyl mixture by 3.8-μm-period gratings.  (a) Liquid crystal confined between gratings at left and between smooth surfaces at right and (b) liquid crystal confined between gratings.

28

Fig. 20. Alignment of MBBA by 3.8-μm-period gratings. (a) MBBA confined between gratings (left) and smooth surfaces (right) and (b) MBBA confined between two gratings (note reverse tilt regions).

(a)

(b)

Surface anisotropy resulting from polishing scratches can be greatly reduced by depositing a layer of some material on the substrate prior to forming the grating structure. Two quartz substrates were coated with a 4200-Å-thick layer of CVD oxide, and 200-Å-deep square-wave gratings were then etched into the CVD layer. The results, shown in Fig. 18, are similar to those from the experiment where the grating was etched directly into the fused quartz, except that the consistent 20° misalignment has been eliminated. In order to estimate the "average" alignment direction in the presence of a Schlieren texture, a photodiode was used to integrate the total light intensity over the microscope field as the sample stage was rotated. The sample was rotated until the minimum light intensity was incident on the photodiode; the diode current was measured using a digital voltmeter with a sampling resistor. At the minimum diode current, the position of the stage was recorded. The photodiode was removed and the stage was repositioned so that the grooves were aligned with the cross hair which indicates the polarization direction. The difference between this latter stage position and the previously recorded position is a measure of the average angular misalignment between the director and the groove direction. Observation of four microscopic fields (each of 5 mm$^2$ area) indicated that the average director was −6°, −9°, +10°, and −9° from the groove direction. This shows that the CVD coating has eliminated the consistent misalignment seen with the uncoated substrates, probably by covering polishing scratches. Also, there is a strong bias toward alignment along the groove direction with the 12-μm-period gratings even though the Schlieren texture interferes with unidirectional alignment.

Why is the 12-μm grating effective at inducing a statistical alignment of the director but highly ineffective at preventing texture formation? What forces act to preserve textures which have a higher distortion energy than the unidirectionally oriented state? The next section considers these issues.

## 3.2 ORIENTED ADSORPTION OF LIQUID CRYSTAL MOLECULES ON SURFACES

One could argue that Schlieren textures nucleate on specific surface defects and that stable textures result because disclinations are pinned on these defects and slight surface anisotropies resulting from polishing scratches, roughness, etc., further control the texture. This seems unlikely since disclinations move during the "growth" of the nematic layer or if the entire layer flows. I will present an alternative model which explains the persistence of textures. Simply stated, liquid crystal molecules adsorb strongly on the surface, and are not free to rotate on the surface unless they are subjected to very large torques. Furthermore, molecules appear to be most likely to adsorb with an orientation corresponding to the orientation of the nematic director in the overlying liquid crystal layer. The adsorbed molecules, in turn, produce torques on the overlying liquid crystal layer, and the bulk nematic tends to orient locally in a direction corresponding to the average direction of the adsorbed molecular layer.

Consider a clean, smooth, amorphous surface which is exposed to the isotropic phase of a liquid crystal. The surface becomes covered with an adsorbed layer of liquid crystal molecules. Molecules are equally likely to adsorb with any surface orientation, though their tilt angle with the surface is well defined. Now, the liquid crystal is cooled to the nematic phase. As soon as a nematic region forms in contact with the surface, the previously adsorbed layer begins to affect the orientation of the overlying bulk liquid crystal. However, immediately after formation of the nematic phase the adsorbed surface layer as a whole is random and exerts no net orienting torque on the overlying liquid crystal. Thus, the initially random adsorbed layer effectively presents a "free surface"; only the tilt angle of the director is specified, and free rotation of the director in the surface plane is possible. Under these conditions a Schlieren texture is free to form as described in the last chapter. If the free surface persisted, all the disclinations would eventually migrate and annihilate each other. However, during the time it takes for the Schlieren texture to disappear, molecules are constantly desorbing from the surface and readsorbing. If the molecules readsorb with a preferred direction, the surface rapidly acquires an anisotropy which stabilizes the overlying layer, allowing further time for adsorption. Our original "free surface" is unstable, and tends to acquire anisotropy. Random textures which form during the growth process are rapidly stabilized by this directional adsorption process.

I have performed experiments to check the "directional adsorption" hypothesis. First, a nematic texture is allowed to stabilize in a "sandwich" between glass substrates. The liquid crystal is heated to the isotropic phase for a brief period, resulting in complete randomization of the bulk liquid crystal, but with insufficient time allowed for appreciable desorption and readsorption on the surface. A strong surface anisotropy should remain when the liquid crystal returns to the nematic phase, favoring the production of a similar texture. If, instead, the liquid crystal were kept isotropic for a prolonged period, the surface should be restored to its original "free surface" condition due to randomization of the adsorbed layer. A new texture would form when the nematic phase is reentered. Figure 21(a) shows a Schlieren texture in an MBBA layer confined between two pieces of Corning 0211 glass. The glass substrates are separated by 50-μm-thick Teflon spacers. The 0211 glass was carefully cleaned using the standard

Fig. 21. (a) Stable MBBA texture; (b) same area after heating to isotropic phase for 30 sec; (c) same area after heating to the isotropic phase for 40 min.

cleaning procedure described in Chap. 2. MBBA was introduced into the sandwich in the isotropic phase and then the sandwich was cooled to room temperature where the nematic phase is stable. The liquid crystal remained at room temperature for 110 min. before the photograph of Fig. 21(a) was taken. Textures become quite stable after 1 to 2 hr, and they show little change if left for several days. The liquid crystal was heated and was kept in the isotropic phase for about 30 sec. After returning to the nematic phase for 36 min. the photo of Fig. 21(b) was taken. Note the striking similarities with Fig. 21(a); essentially the same texture has formed. The liquid crystal was then heated to the isotropic phase for 40 min. and was cooled to the nematic phase. After the liquid crystal sat in the nematic phase for 20 min., the photo of Fig. 21(c) was taken. The main features of the texture are completely different from those of Figs. 21(a) and (b).

As a further test of the adsorption hypothesis, an experiment was performed to see if liquid crystal layers aligned by strong electric fields will leave an aligned adsorbed layer which can survive brief heating above the isotropic-nematic transition temperature. A sandwich of two pieces of Corning 0211 glass separated by 50-μm-thick spacers was constructed. The spacers were pieces of steel "feeler stock," and wires were connected to the spacers using silver paint. The straight edges of the spacers were aligned and were separated by a 1-mm gap. Thus, a voltage could be applied across the gap producing an electric field which lies nearly in the plane of the glass substrates. The heptyl/butyl mixture, which has a large positive dielectric anisotropy and tends to align along the electric field lines was used in the sandwich.

Figure 22(a) shows the liquid crystal layer in the nematic phase, before the application of any electric fields. The texture is "random" and the average brightness does not change as the layer is rotated between crossed polarizers. There is no "preferred" orientation of the director. A potential of 1 kV was then applied between the spacers for 1 hr. Figures 22(b) and (c) show the layer after exposure to the field, which strongly aligned the bulk liquid crystal. The cross hair in the photo shows the polarization directions of the polarizer and analyzer. In Fig. 22(b),



(a)

(b)

(c)
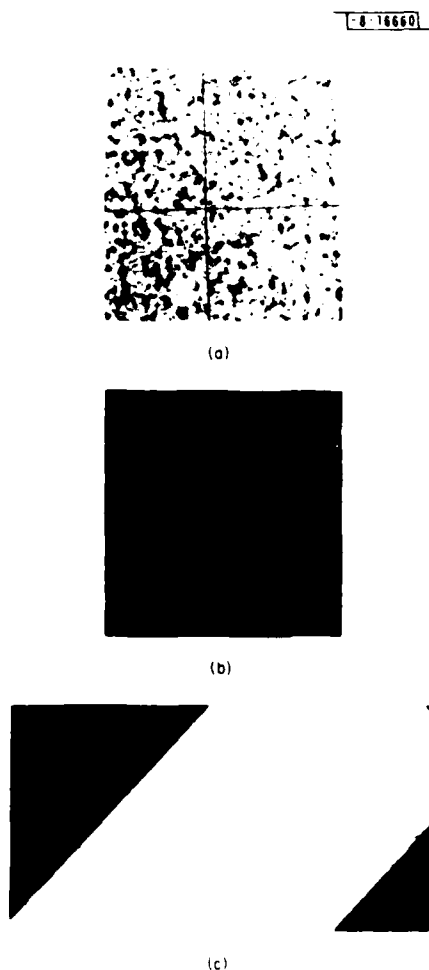
Fig. 22. (a) Texture of heptyl/butyl mixture before application of electric field; (b) and (c) same area after the field was turned off. (b) and (c) show two different orientations with respect to the microscope polarizers.

the electrode edges (the black field boundaries) are parallel to a cross-hair line, whereas in Fig. 22(c) the electrode edges are at about 45° to the cross hairs. Note that the liquid crystal layer looks darker in Fig. 22(b) than in (a), but that it is lighter in Fig. 22(c) than in (a). The exposure time was identical for all three photos. This picture sequence shows that the director has become appreciably aligned by the electric field. It should be noted that, first, the photos were taken with the electric field turned off and that the alignment seems to persist indefinitely after removal of the aligning field and, second, 30 sec. of heating to the isotropic phase does not destroy the alignment effect. This indicates that an anisotropic layer of adsorbed molecules was formed during prolonged contact with the oriented nematic phase.

### 3.3 EFFECTS OF SQUARE-WAVE GRATINGS ON THE GROWTH OF NEMATIC THIN FILMS – EXPLANATION OF MAXIMUM PERIODICITY FOR GOOD ALIGNMENT

Other authors[10-12] have derived formulas which estimate the energy per unit area required to misalign a nematic layer in contact with a grating structure. For instance, Berreman calculates:

$$\Delta F = \frac{1}{4} k_{11} A^2 \left(\frac{2\pi}{P}\right)^3 \quad . \tag{3-1}$$

The nematic director is assumed to lie tangent to the surface at all points. $\Delta F$ is the free energy required to deform the liquid crystal from its undistorted state with the director lying along the grooves to a state where the director is perpendicular to the groove direction but tangent to the surface at all points on the surface. The grating is assumed to be sinusoidal, with amplitude A and a period P. Two simplifying assumptions are needed to obtain this simple analytical result. First, it is assumed that the three elastic constants of the liquid crystal are equal which is not a very good assumption; $k_{11}$ in Eq. (3-1) represents this single elastic constant. Second, the director at the grating surface must be deformed only slightly from the uniform orientation parallel to the surface which exists some distance away from the surface in the bulk liquid crystal. In other words, P must be much greater than A for the formula to be meaningful. For square-wave gratings, the director would have a 90° bend at the top and bottom corners of the gratings, and Berreman's solution becomes inapplicable.

Solving the nonlinear elastic continuum equation for the case of square-wave grating boundary conditions is mathematically difficult, and may not prove particularly illuminating. Instead, I will present some ideas here which at least give some insight into the alignment forces generated by a square-wave grating, though I will not attempt to solve the continuum elastic equation.

If the nematic director were forced to lie perpendicular to the groove direction and parallel to the substrate surface everywhere on the surface, 90° discontinuities in the director orientation would occur at the top and bottom corners of the grooves. This represents an impulse in the divergence of the director field at these corners. The distortion energy associated with such discontinuities is infinite. We can conclude from this that no matter what the orientation of the overlying nematic layer may be (at some distance from the surface), tremendous forces (limited only by the radius of curvature of the corners in the grating or by the fact that "tight binding" of the surface layer cannot be assumed if the forces become excessive) keep the director pointing along the groove direction at the corners. Thus, the appropriate way to view the square-wave grating alignment force is not in terms of the energy required to completely align the surface layer of the liquid crystal perpendicular to the grooves, which would be infinite. Instead,
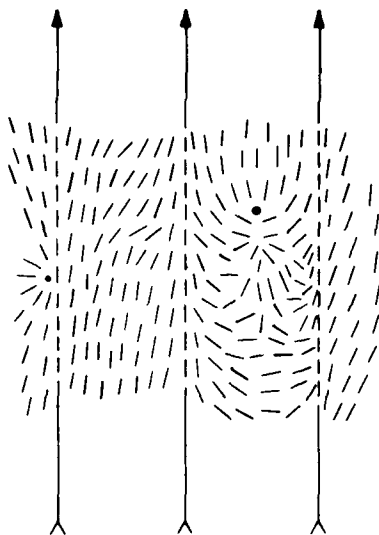
Fig. 23. Sketch showing schematically that square-wave grating corners produce "line" boundaries where the nematic director is constrained to lie along the groove direction. Away from the corners the director orientation may be changed.

one can argue that the director is forced to lie along the grooves at the corners of the square wave, but that it may be distorted as one moves away from the corners, as shown in Fig. 23. Note that the situation sketched in Fig. 23 looks very much like a cross-sectional view of a tunable birefringence cell, except that the director is constrained at line boundaries rather than planes. The director is constrained at the equally spaced lines, but in between these lines the liquid crystal can be distorted by surface forces or by electric fields. The magnitude of the alignment force exerted by these line boundaries on the liquid crystal at the surface midway between the lines can be estimated by treating the line boundaries as planes, which makes the problem one-dimensional and identical to the case of tunable birefringence or twisted nematic cells.

The torque exerted by the boundaries of a tunable birefringence cell on the liquid crystal in the middle of the cell is proportional to the magnitude of the elastic constants and inversely proportional to the cell thickness. Thus, the torque produced by the grating "corners" acting to align the surface layer in between the corners will increase linearly with the grating spatial frequency. The cutoff periodicity for alignment of the heptyl/butyl mixture is approximately 4 μm, but the spacing between "corners" is half of that, or 2 μm. This is roughly equivalent to saying that the surface adsorption forces which can maintain misalignment are equivalent to forces required to deform the liquid crystal in the middle of a 2-μm-thick tunable birefringence cell. In the literature we find that the voltage required to deform the liquid crystal in the center of a 12-μm-thick twisted nematic cell containing the heptyl/butyl mixture is about 2 V (Ref. 34). This corresponds to an electric field of about $1.6 \times 10^5$ V/m. The field required for a 2-μm-thick cell would be about $9.6 \times 10^5$ V/m. This compares surprisingly well with the $10^6$ V/m required to realign the adsorbed layer by means of an electric field in the experiment described in Sec. 3.2. This simplified view also suggests that with heptyl/butyl liquid crystal sandwiches greater than about 2 μm thick, the torque exerted by the liquid crystal at one substrate may be inadequate to

34

bring the liquid crystal layer at the other substrate into alignment. This is consistent with experimental evidence; 50-$\mu$m-thick layers of the heptyl/butyl mixture between 2 smooth quartz surfaces show many domains which undergo a twist between the quartz substrates.

In closing this chapter I would like to address the issue of whether the results obtained here with a limited number of liquid crystals and with a fixed groove depth can be generalized.

The groove depth is not likely to be important over a fairly wide range of variation. As discussed earlier, the aligning effect of the groove is probably due almost entirely to the corners. As long as the corners at the top and bottom of the grooves are spaced close together relative to the grating period, their exact spacing should be unimportant. This is similar to saying that two closely spaced point charges can be lumped into an equivalent charge if only the far field is examined.

The alignment forces generated by the grating also increase linearly as the elastic constants of the liquid crystal increase. One can argue, however, that all nematic liquid crystals with a nematic-isotropic transition temperature near room temperature should have nearly equal elastic constants. The mean field theory of liquid crystal phase transitions[35] states that the nematic-isotropic transition temperature in degrees Kelvin is proportional only to the strength of the intermolecular force. The elastic constants should also be proportional to the strength of the intermolecular force. Thus, it is unlikely that substantial variations in the elastic constants will be found among room-temperature nematics, which generally have their transition temperatures near room temperature.

Considerable variation might exist in the adsorption forces which must be overcome to produce unidirectional alignment. The work of adhesion, which is related to the contact angle and the surface tension of the liquid crystal, may be a predictor of the directional adsorption forces, and thus of the periodicity required to produce alignment. One would think that liquid crystal/substrate combinations could be found where the directional adsorption forces could be reduced.

In summary, square-wave gratings with periods below about 5 $\mu$m are required to produce good alignment of the room-temperature nematics which I have used. This is consistent with the results of Wolff et al.[12] who found that 1-$\mu$m-wide grooves produced by scribing with a diamond stylus had to be placed closer than about every 10 $\mu$m to produce good alignment of nematics.

The smectic A phase of M24 was also aligned using 3200-Å-period gratings. In the grating area the liquid crystal was uniformly aligned, and only very faint striations were visible in the layer. Outside the grating area, a pronounced texture with focal conics and fan-shaped defects was evident. The quality of alignment produced by the 3200-Å-period gratings is better than with plates prepared by oblique evaporation of silicon monoxide. Gratings may be the best way to produce uniform alignment of smectic phases.

# CHAPTER 4
## APPLICATIONS OF PLANAR TECHNOLOGY TO LIQUID CRYSTAL ALIGNMENT

### 4.1 ALIGNMENT OF MBBA BY A GRATING PATTERN IN AN ORGANIC MONOLAYER

In previous chapters I have discussed the mechanism by which surface relief structures align liquid crystals. The relief structure in effect presents spatially varying boundary conditions to the liquid crystal layer. Spatial variation in the boundary conditions could be achieved in another manner. By changing the surface material which is in contact with the liquid crystal, boundary conditions such as the tilt angle can be altered, as discussed in Chap.2. I will now describe an experiment where a grating structure which had no appreciable surface relief but presented spatially varying tilt boundary conditions was fabricated and used to align liquid crystals.

Figure 24 illustrates the procedure used to produce the structure. Twelve-micrometer-period square-wave gratings consisting of 300-Å-thick chromium lines were fabricated on fused
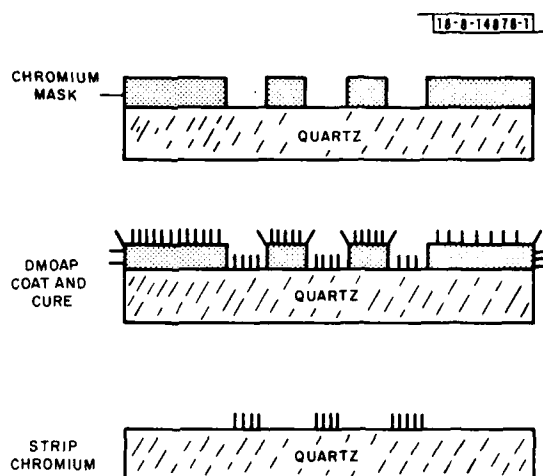


Fig. 24. Procedure used to form patterned layers of DMOAP.

quartz substrates. The substrates were coated with the silane coupling agent DMOAP and the DMOAP layer was bonded to the substrate by a baking process (see Appendix A). The chromium lines were then stripped in a chemical etchant, leaving a pattern of DMOAP lines alternating with clean quartz lines. The DMOAP coating should be only a monolayer thick.[6] Thus, after removal of the chromium no appreciable surface-relief structure exists. However, the liquid crystal will prefer to align with a homeotropic orientation over the DMOAP-coated regions and with a nearly parallel orientation over the clean quartz.

Figure 25 shows photos of an MBBA layer viewed orthoscopically between crossed polarizers. The layer is 50 μm thick and the top substrate is coated uniformly with DMOAP while the bottom substrate was prepared with a DMOAP grating pattern as described above. The area

(a)

(b)



(c)
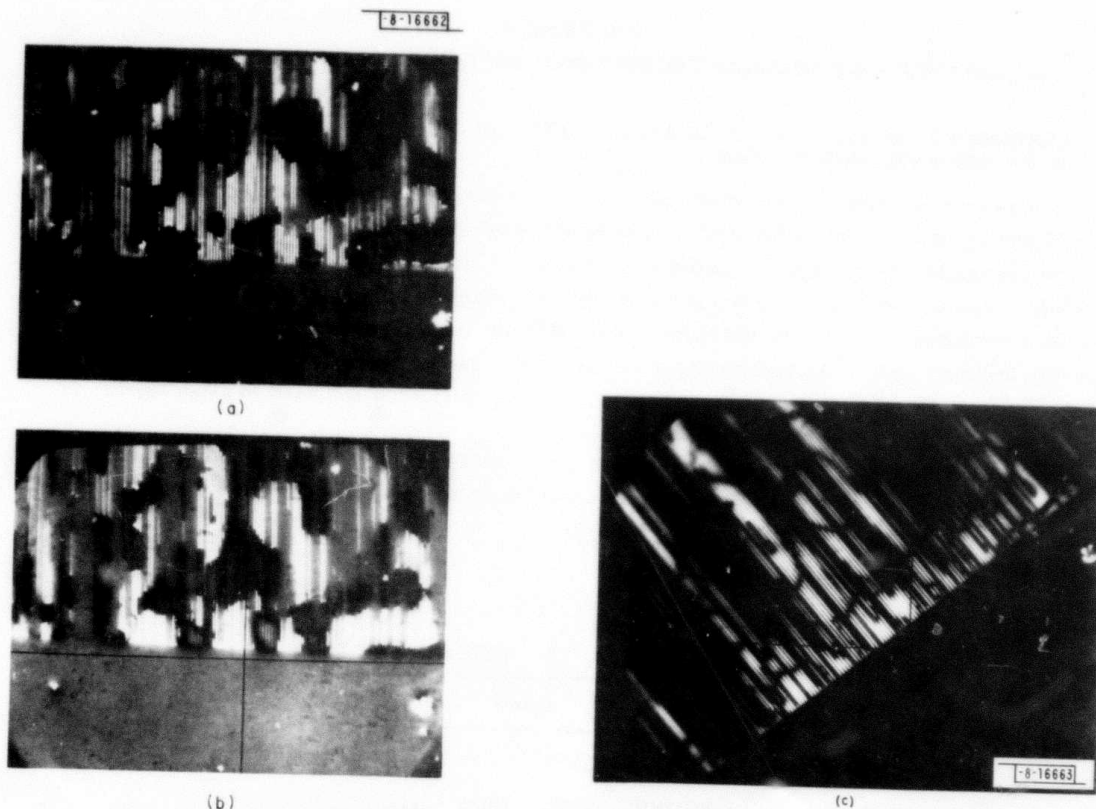
Fig. 25.   MBBA layer aligned by patterned surface layer of DMOAP.   (a) and
(b) show the MBBA illuminated with light which is not normally incident on the
layer; this contrasts regions of reverse tilt.   (c) Same area as (a) and (b), but
with normally incident illumination and DMOAP lines oriented at 45° to the po-
larizer directions.

outside the grating is uniformly coated with DMOAP.   When the grating grooves were aligned
parallel or perpendicular to the direction of the incident polarization,  the entire field of view
appeared dark.   As shown in Fig. 25(c),  clearly visible bright lines appear when the grooves
are oriented at 45° to the polarizer directions,  shown by the cross hairs in the photo.   Thus,
the liquid crystal over the clean quartz stripes has become oriented along (or perpendicular to)
the direction of the DMOAP lines.   Figures 25(a) and (b) were taken with light incident at a
slight tilt along the direction of the lines and to either side of the substrate normal.   This indi-
cates that the dark lines in Fig. 25(c) separate regions of reverse tilt, because patches which
appear dark in Fig. 25(a) appear light in (b) and vice versa.   No contrasting patches are seen if
the incidence angle of the light is varied in the orthogonal plane.   One can conclude therefore that
the director is aligned along the DMOAP lines and forms a tilt angle with the substrate.

The above experiment demonstrates that patterned organic layers can be used to control the
alignment of liquid crystals.

38

## 4.2 APPLICATION OF SURFACE-RELIEF STRUCTURES FABRICATED BY THE PLANAR PROCESS TO LIQUID CRYSTAL DISPLAYS

The twisted nematic liquid crystal display is used commercially in such devices as wrist-watches, calculators, and in other applications where display devices with low-cost, low-power dissipation, low weight, and good readability in high ambient light levels are needed. The operation of twisted nematic displays has been described by several authors,[36,37] but the basic principles will be reviewed here.

Two transparent substrates are first coated with a thin layer of material, such as tin oxide, which is a transparent conductor. The tin-oxide layer is then made anisotropic by unidirectionally rubbing with abrasives or by obliquely evaporating a thin silicon-monoxide layer on top of it. The substrates will now produce unidirectional alignment of a nematic layer along the axis of anisotropy and in the surface plane. The substrates are then assembled into a sandwich similar to the one shown in Fig.3, except that the substrates are aligned so that the nematic director orientation will be orthogonal at the two substrate surfaces, with a smooth twist of the director in the intervening bulk nematic. The sandwich is filled with a liquid crystal that has positive dielectric anisotropy. The substrates containing the twisted nematic layer are then placed between crossed polarizers, with the nematic director at the substrate surfaces oriented either parallel or perpendicular to the direction of polarization of the polarizers.

This structure can be used as a light valve. Light passing through the first polarizer becomes linearly polarized and becomes either a pure ordinary or extraordinary wave upon entering the liquid crystal. For thick enough nematic layers, the twist of the director between top and bottom surfaces takes place slowly enough so that the polarization of the light tends to "follow" the twist, and the polarization of the incident light is rotated by 90°. For good rotation the cell thickness must be much greater than $\lambda/\Delta n$, where $\lambda$ is the wavelength of the light and $\Delta n$ is the birefringence of the liquid crystal. Thus, cell thicknesses of at least 10 $\mu$m are usually required. The polarization tends to rotate because the phase velocities for the ordinary and extraordinary waves are different, and with a slowly twisting layer, we have only weak coupling between the two modes. In such a situation, where two weakly coupled modes are not "phase matched," power transfer between the modes becomes very inefficient; this problem is well known to those who use crystals for harmonic generation with lasers. Thus, power introduced as an ordinary wave tends to remain an ordinary wave, but the direction of polarization corresponding to the ordinary polarization varies with the twist in the liquid crystal. The light which passes through the layer has been rotated in polarization, and consequently passes through the second polarizer. Our light valve is "on" in the rest state.

If a voltage is applied between the tin-oxide layers, the liquid crystal director will tend to point normal to the substrates, along the electric field lines. Light passing through the first polarizer no longer sees a twisted nematic, and passes through the layer with little change in polarization. This light is absorbed by the second polarizer, so the light valve is "off."

The structure shown in Fig.26 is a twisted nematic display of extraordinary simplicity fabricated using submicrometer grating technology. Gold lines of 1000-Å thickness and 3200-Å period were fabricated on two pieces of 225-$\mu$m-thick Corning 0211 glass. The pieces of glass were assembled into a sandwich with the gold lines on the inside and with the substrates oriented so that the gold lines were orthogonal. The sandwich was filled with the heptyl/butyl mixture. The spacers kept the substrates 12 $\mu$m apart. The gold lines were interconnected at the edge of the grating by a continuous gold film, and an aluminum foil contact was connected to the gold layer of each substrate.
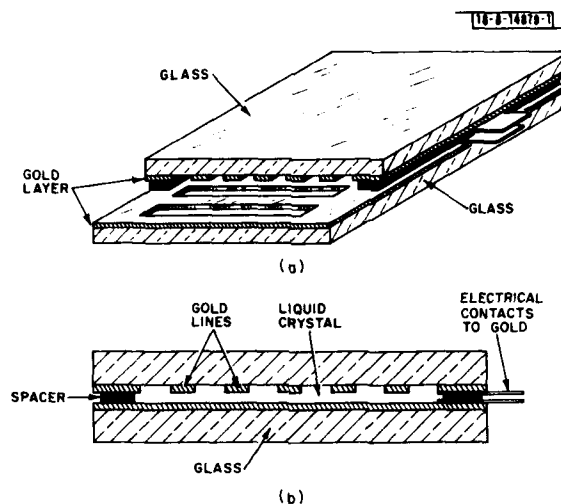
Fig. 26. Twisted nematic liquid crystal display made with metallic
gratings. (a) Three-dimensional view and (b) cross-sectional view.

This very simple structure provides all the basic elements of a twisted nematic display. First, the gold lines provide orthogonally oriented surface-relief structures which are effective at aligning the liquid crystal. Second, since the grating consists of conducting parallel wires spaced closer than the wavelength of visible light, it will act as an optical polarizer. The two gratings constitute a pair of crossed polarizers, and they are automatically properly aligned with the liquid crystal layer optic axis. Third, the spacing of the substrates is much greater than the spacing of the gold lines. For low frequencies, the gold gratings act as conducting parallel plates since the fringing fields of the wires decay within a few thousand angstroms from the surface. About 3 V were required to "cut off" the light transmission in this display.

| TABLE III |
|---|
| GOLD GRATINGS PREPARED BY ION-BEAM ETCHING 700-Å-THICK GOLD LAYER USING HOLOGRAPHICALLY EXPOSED AZ-1350 RESIST MASK |

Infrared Measurements:

| Wavelength (μm) | P |
|---|---|
| 2.5 | 0.06 |
| 3.33 | 0.015 |
| 4.55 | <0.0025 |

Visible Measurements:

P = 10 at a wavelength of 6328 Å

P = polarization ratio = transmitted intensity for E parallel to wires/transmission for E perpendicular.

This novel method of making a twisted nematic display may have real advantages, in addition to demonstrating an interesting application of submicrometer grating technology. First, the structure is very simple and has a minimum number of elements, so it could potentially be made at extremely low cost. Second, metal grating polarizers are not subject to degradation if exposed to extremes of temperature or humidity; the deterioration of conventional plastic sheet polarizers in harsh environments has been a problem for liquid crystal display users.

A few comments should be made about the polarizing properties of metal gratings, though a complete presentation of all the data which I have collected would represent a substantial digression and is beyond the scope of this report. Hertz discovered in his early experiments with radio waves that gratings of thin wires would polarize the radiation. Bird and Parrish[38] have produced wire grating polarizers which are effective in the near infrared, substantially extending the spectral range of wire grid polarizers. The theory of wire grating polarizers is reviewed in an article by Larsen.[39] The theory is simple for periodic arrays of perfectly conducting cylindrical wires whose diameters are much less than the grating period, and when the grating period is much less than the wavelength of the radiation. Under these conditions almost complete transmission through the grating can occur for a normally incident plane wave with its electric field polarized perpendicular to the wires, whereas nearly complete reflection occurs when the polarization is parallel to the wires.

Tables III and IV summarize the infrared and visible region performance of polarizers which I fabricated. All polarizers consisted of 3200-Å-period gratings of metal lines on 225-μm-thick Corning 0211 glass substrates. The metal lines had widths which were about half of the period and thicknesses ranging from 500 to 1000 Å. Excellent polarization properties consistent with the theory described above were obtained in the infrared. A Beckman IR-4250 spectrophotometer was used for the measurements; the light source was polarized either by using a Perkin-Elmer wire grating polarizer or another one of my polarizers, with similar results.

In the visible part of the spectrum relatively poor performance and poor agreement with the theory might be expected on several grounds: (a) The grating period used is no longer much less

| TABLE IV |
| --- |
| GRATINGS PREPARED BY LIFTOFF OF 900 Å OF ALUMINUM EVAPORATED OVER X-RAY EXPOSED GRATING IN PMMA |

Infrared Measurements:

P < 0.01 for wavelengths greater than 2.5 μm

Visible Measurements:

| Wavelength (nm) | P |
| --- | --- |
| 800 | 0.16 |
| 700 | 0.19 |
| 600 | 0.24 |
| 500 | 0.68 |

P = polarization ratio = transmitted intensity for E parallel to wires/transmission for E perpendicular.

than the wavelength, (b) the wire diameter is not much less than the period, and (c) metals can hardly be considered perfect conductors at optical frequencies. The yellow color of gold indicates that its reflectivity is frequency dependent, and gold is only about 87 percent reflective (at 6328 Å), vs 100 percent for a perfect conductor. Alkali metals become transparent in the near UV as the plasma frequency of the conduction electrons is exceeded. In short, metals are hardly classical conductors at optical frequencies and the simple theory of wire grating polarizers may not apply.

Aluminum gratings fabricated by liftoff behaved as expected, producing a weakly polarized beam, and transmitting more light polarized perpendicular to the wires. A very surprising result was obtained with the gold gratings in the visible region. Light was strongly polarized by the grating, and the polarizing effect was opposite from that predicted by the theory. More light polarized parallel to the wires is transmitted than light polarized perpendicular. Table V gives some further data on the optical properties of gold grating polarizers.

The performance of liquid crystal displays with grating optical polarizers is limited by the contrast ratio that can be obtained with the polarizers. Using the gold gratings, which exhibit unexpectedly good polarizing properties, contrast ratios of 10:1 between the "on" and "off" states have been obtained for liquid crystal displays used as light valves. The performance of the polarizers might be improved if gratings of finer spatial periods were produced.

| TABLE V | | |
|---|---|---|
| TRANSMISSION AND REFLECTION OF HELIUM-NEON LASER LIGHT FOR 3200-Å-PERIOD GOLD GRATING POLARIZERS | | |
| | Transmitted Power (percent) | Reflected Power (percent) |
| E parallel to grating lines | 22 | 58 |
| E perpendicular to grating lines | 2.2 | 71 |
| No grating, continuous film | 0.46 | 86 |
| Wavelength of light is 6328 Å. Plane wave arrives at 0.9° from normal incidence. | | |

# CHAPTER 5
# THE FUTURE

## 5.1 SUGGESTIONS FOR FURTHER WORK

This report has only begun to explore the possibilities opened by the ability to control liquid crystal thin film orientation using well-controlled surface structures. Submicrometer-period gratings produce high-quality, stable, unidirectional alignment of nematic phases. Smectic A phases can be aligned with fewer defects by 3200-Å-period square-wave gratings than by other current surface treatment methods. Though submicrometer periodicity gratings are not required for alignment of nematic phases, the alignment quality improves radically as submicrometer dimensions are approached.

Further work is clearly needed to understand fully the properties of wire grating polarizers in the visible part of the spectrum and to improve their characteristics.

Using a "planar" fabrication method, as described in this report, it should be possible to produce complex patterns of liquid crystal alignment at will. A very exciting possibility is that patterns of alignment produced in nematic liquids might be "frozen in" to a solid phase. Nematic MBBA can be quenched by rapid cooling to liquid nitrogen temperatures into a glassy phase which retains the nematic ordering.[40-42] Kessler and Raynes[42] present evidence that a twisted nematic layer oriented by rubbed surfaces retains its ordering when cooled to a glassy phase. These authors used liquid crystals with room-temperature nematic phases. The glassy phase is meta-stable and converts spontaneously to the crystalline state at a temperature below the melting point of the crystal. If glassy phases could be produced from nematic liquid crystals whose melting points are substantially higher than room temperature, it would be possible to produce useful solids with nematic ordering which are stable at room temperature. Surface structures would be used to orient the high-temperature nematic phase in the desired manner before quenching to room temperature. A twisted nematic solid glass layer produced in such a manner would provide a low-cost optical component capable of efficient 90° polarization rotation. Other applications can be envisioned.

This represents only the first step toward engineering the structure of solid or liquid organic layers.

# APPENDIX A
# FABRICATION TECHNIQUES

## A.1 PLANAR FABRICATION TECHNIQUES FOR SURFACE GRATINGS

The majority of the techniques used to fabricate the surface gratings for these experiments have been described elsewhere. In his PhD. thesis Flanders[5] describes holographic exposure, X-ray exposure, liftoff, and reactive-ion etching techniques currently used at M.I.T. Lincoln Laboratory. A recent article[43] also provides fabrication information for submicrometer periodicity gratings. The reader is referred to these sources for background information on microfabrication methods.

The 3200-Å-period square-wave gratings etched into fused quartz were prepared by the process illustrated schematically in Fig. A-1, and described in detail in Ref. 43. All quartz substrates used in these experiments were Optosil 2;* they had a commercial-grade polish which typically corresponds to a surface roughness of <1 μ-in. Cerium oxide on a felt lap was used for polishing.
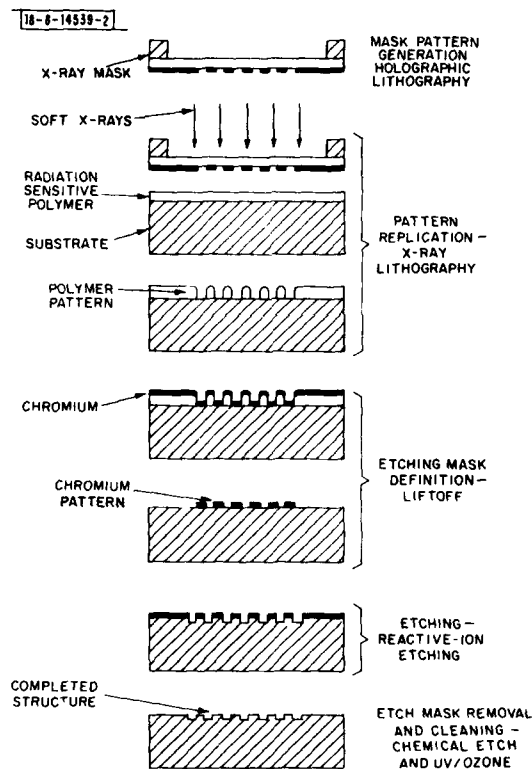


Fig. A-1. Fabrication process for 3200-Å-period gratings.

Cu-L soft X-ray lithography was used to expose 3200-Å-period gratings in a layer of polymethyl methacrylate (PMMA) on the fused quartz. This produces a grating in the PMMA resist with smooth, vertical sidewalls suitable for liftoff. 200 Å of chromium was evaporated onto the

---

*Optosil 2, Amersil, Inc., Sayreville, New Jersey.

45

substrates at normal incidence. "Liftoff" was then performed by dissolving the PMMA in chloro-benzene. The grating of chromium lines was then used as an etch mask during reactive-ion etching[44,43] of the quartz in $CHF_3$ gas. The total etching time was 1 min., which produces an etch depth of about 200 Å in our system. After reactive-ion etching, the substrates were UV/ozone cleaned[30] and the chromium was removed using Kodak chromium etch.[*] The chromium is very difficult to remove after the reactive-ion etching, and UV/ozone cleaning is needed to improve the etch rate of the chromium and insure complete removal of the mask.



Fig. A-2. Grating (3200-Å-period) etched into silicon dioxide which was grown by thermal oxidation of a silicon wafer.

Figure A-2 shows a 3200-Å-period square-wave grating etched in fused quartz using the fabrication techniques described above. However, this sample was etched to a greater depth to facilitate viewing in the scanning electron microscope (SEM). Note that straight, nearly verti-cal sidewalls are obtained by reactive-ion etching. Measurements from SEM photos show that the sidewalls are within 6° of the vertical. Good-quality square-wave gratings with submicro-meter periods cannot be obtained by aqueous chemical etching because the etching process is isotropic and tends to undercut the mask while etching into the substrate, producing sloped side-walls. Ion-beam etching is highly directional and does not produce undercutting; however, re-deposit onto the sidewalls of substrate material dislodged by the ion beam degrades the etch profile. No attempts have been made to align liquid crystals using gratings etched by aqueous chemical or ion-beam etching. Such experiments would be very interesting, however.

Reactive-ion etching produces highly directional etching and is free of problems of redo-posit of material removed from the substrate. Furthermore, the ratio between the etch rate of the quartz and the etch rate of the chromium mask is greater than for ion-beam etching. This reduces the thickness of the mask required to etch to a specified depth without problems from faceting of the mask caused by the ion-bombardment. Reactive-ion etching is performed in a standard MRC[†] sputtering system. The substrates are placed on a quartz plate on top of the

[*] Formula suggested by Kodak for etching chromium plates: 164.5 g ceric ammonium nitrate and 43 ml perchloric acid; add deionized water to make 1 liter.

[†] Materials Research Corporation.

RF electrode of the system. This electrode "self-biases" to a DC potential a few hundred volts negative with respect to the plasma in the chamber. Ion-bombardment of the substrates at nearly normal incidence takes place. The reactive-ion etching process appears to involve chemical reactions with reactive species generated in the $CHF_3$ plasma, producing a volatile reaction product which does not redeposit. Furthermore, the reaction rates are greatly increased in the regions exposed to ion-bombardment. Reactive-ion etching is a key step for producing square-wave gratings with sharp corners and vertical sidewalls in fused quartz substrates.

The gratings of 1-, 3.8-, and 12-μm periodicity were all produced by reactive-ion etching using a chromium mask. The method of generating the mask was somewhat different in these cases, however. Clean quartz substrates were first coated with 300 Å of chromium, using electron beam evaporation. For the 1-μm-period gratings, the chromium was covered with 1000 Å of AZ-1350J photoresist which was then exposed using holographic lithography (argon laser, wavelength = 4579 Å, beams incident at 13.4° from the substrate normal). For the 3.8- and 12-μm gratings, the chromium was covered with 5000 Å of AZ-1350B resist; grating patterns were then exposed using conformable photomask lithography.[45] The photomasks were replicas of masters generated using a Mann 1600 pattern generator and a Mann 1795 photorepeater.

After exposure and development of the photoresist, the chromium layer was etched for 20 sec in Kodak chromium etch. The resist was then stripped by rinsing the substrates in acetone.

After reactive-ion etching and chromium mask removal, all substrates were cleaned using the standard procedure described in Chap. 2.

## A.2  DMOAP COATING OF SUBSTRATES

The procedure used to coat substrates with a monolayer of DMOAP* was developed by Kahn.[1,6] It is reproduced here:

(a)  Mix up a 0.1% solution, by volume, of DMOAP in deionized water.

(b)  Immerse the substrates to be coated in the solution for 5 min. Maintain gentle agitation.

(c)  Remove the substrates and rinse under flowing room-temperature deionized water for 1 to 2 min. to remove excess DMOAP. The substrates should now be very poorly wetted by water.

(d)  Blow dry substrates with dry nitrogen.

(e)  Bake the substrates at 110° for 1 hr.

---

* DMOAP is N,N-dimethyl-N-octadecyl-3-aminopropyltrimethoxysilyl chloride; available from Dow Corning, Midland, Michigan, as silane XZ-2230.

# APPENDIX B
## TECHNIQUES USED TO DETERMINE THE ORIENTATION,
## INCLUDING TILT FROM THE SUBSTRATE, OF THE NEMATIC DIRECTOR

### B.1 ORTHOSCOPIC OBSERVATION BETWEEN CROSSED POLARIZERS

This is conventional transmission optical microscopy except that the light incident on the specimen is linearly polarized and must pass through another crossed polarizer after passing through the sample. The liquid crystal layer is in one of the focal planes of the microscope. The substage condenser is adjusted to produce a reasonably parallel beam of light, which arrives at normal incidence to the liquid crystal layer. The specimen stage permits rotation of the liquid crystal layer with respect to the polarization direction of the incident light. White light from an incandescent source is generally used.

Consider a liquid crystal layer which is uniformly aligned and whose nematic director has tilt with respect to the substrate plane. This is a thin slab of uniaxial material with the optic in the direction of the nematic director. Figure B-1 shows the slab; the coordinate system is chosen so that the optic axis lies in the y-z plane and the incident light will be linearly polarized with its E-field in the x-y plane. The optic axis forms a tilt $\theta$ with the substrate plane.
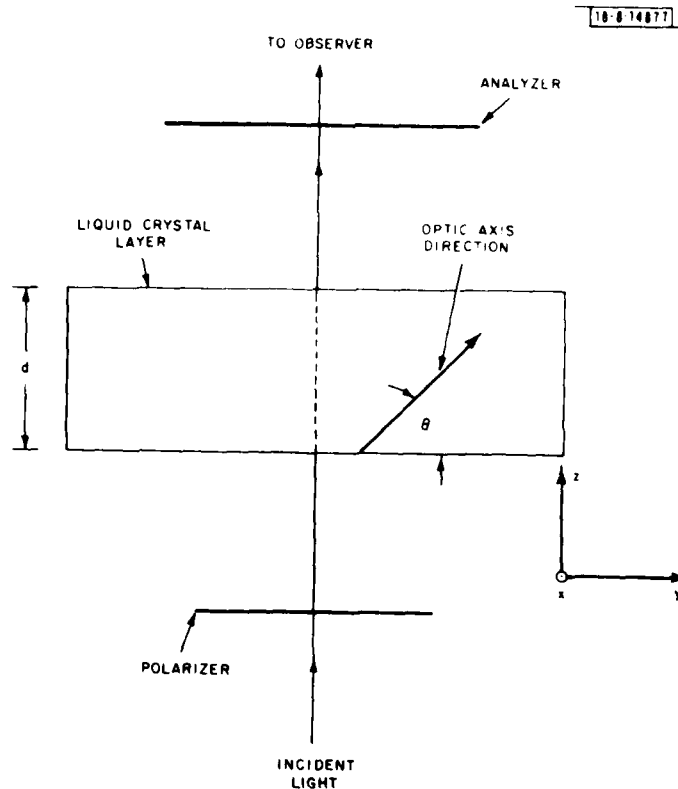


Fig. B-1. A liquid crystal layer between crossed polarizers with normally incident illumination.

49

Light which is polarized perpendicular to the optic axis (the x direction) will produce only an ordinary wave in the liquid crystal layer. Light polarized in the direction of the optic axis projection on the substrate plane (the y direction) will produce only an extraordinary wave. In either case, light incident on the liquid crystal will remain linearly polarized in the same direction after passing through the layer, and will be absorbed by the crossed analyzer, resulting in a dark field of view.

For light which is not polarized perpendicular to the optic axis or parallel to its projection, both an ordinary and extraordinary wave will be produced. The ordinary k-vector magnitude is

$$k_o = \frac{2\pi}{\lambda_o} n_o \tag{B-1}$$

and the extraordinary wave k-vector magnitude is

$$k_e = \frac{2\pi}{\lambda_o} n \tag{B-2}$$

where $\lambda_o$ is the wavelength of the light wave in free space, and $n_o$ is the ordinary index of the medium. $n = n(\theta)$ is the effective extraordinary index, where

$$n^2 = \frac{n_o^2 n_e^2}{n_e^2 \sin^2 \theta + n_o^2 \cos^2 \theta} \tag{B-3}$$

and $n_e$ is the extraordinary index of the medium.

In the case where both ordinary and extraordinary waves exist, the light wave leaving the medium will have the same polarization as the incident wave only if the ordinary and extraordinary waves remain in phase. That is, we require

$$k_e d - k_o d = 2\pi m \tag{B-4}$$

where m is an integer. This is equivalent to

$$\frac{d}{\lambda_o} (n - n_o) = m \quad . \tag{B-5}$$

For white light, where a continuous range of values of $\lambda_o$ exists, Eq. (B-5) cannot be satisfied simultaneously at all wavelengths, except if $n = n_o$. $n = n_o$ implies either (a) the medium is isotropic, or (b) $\theta = 90°$, that is the liquid crystal layer is homeotropic.

Thus, orthoscopic examination with white light of liquid crystal layers between crossed polarizers has the following properties:

(a) If the layer is isotropic or homeotropic, the extraordinary wave is degenerate and the layer will appear dark for all rotations of the sample in the x-y plane.

(b) If $\theta \neq 90°$, then the layer will appear dark only when the incident polarization is perpendicular to the nematic director or parallel to its projection on the x-y (substrate) plane.

(c) If d is small or $n_e - n_o$ is small or the liquid crystal is nearly homeotropic, interference colors will be observed. The progression of colors observed can be found in tables such as in Ref. 46.

(d)  If the nematic director is not uniformly oriented (but does not undergo
a twist between the upper and lower substrates), then black lines will
be visible in the nematic layer showing all regions where the director
projection is parallel or perpendicular to the incident polarization.
Thus, the nematic director orientation is easily visualized using this
technique.

(e)  If the liquid crystal director twists between the upper and lower sub-
strates, there will not be any orientation of the sample in the x-y
plane for which the incident white light remains linearly polarized
without undergoing a rotation of the polarization direction.  The sam-
ple will never appear dark between crossed polarizers, but if the
angle between the polarizer and analyzer is adjusted, pronounced nulls
in the transmission can be obtained.  Thus twist is easily detected.

## B.2  TILT-ANGLE ESTIMATES USING WEDGE-SHAPED NEMATIC LAYERS

If one spacer is removed from the liquid crystal sandwich shown in Fig. 3 of Chap. 2, a
liquid crystal layer of linearly varying thickness will be formed.  The thickness change is typi-
cally 50 $\mu$m over a distance of about 2 cm, which corresponds to a 0.14° tilt between the sub-
strates.  Thus, the substrate planes remain essentially parallel, and the effect of the tilt of
the substrates on the alignment of the liquid crystal can be neglected.

If a beam of monochromatic light passes through the nematic layer at normal incidence as
in Fig. B-1, and if the incident polarization is at 45° to the y axis, then both an ordinary and
an extraordinary wave will be excited in the liquid crystal.  As discussed in Sec. B.1 of this
appendix, the liquid crystal layer will appear black only when

$$t(x, y) \ \frac{(n - n_o)}{\lambda_o} = m \tag{B-6}$$

where $t(x, y)$ is the thickness of the layer.

With a linear thickness variation, equally spaced black fringes will occur when Eq. (B-6) is
satisfied.

The effective birefringence, $n - n_o$, which is a function of the tilt angle is easily determined
if the spacing between the dark fringes is measured

$$\Delta n = n - n_o = \frac{\lambda_o}{S \Delta \ell} \tag{B-7}$$

where

  S = slope between substrates,

  = spacer thickness/length of wedge, and

  $\Delta \ell$ = spacing between fringes.

It turns out that this method has already been proposed by Haller et al.[47] for birefringence mea-
surements and gives excellent results.

Once the effective birefringence is known, the calculation of the tilt angle is straightforward. Using Eq. (B-3) we get

$$\theta = \cos^{-1}\left[ \frac{\Delta n(2n_o + \Delta n) \, n_e^2}{(n_e^2 - n_o^2)(n_o + \Delta n)^2} \right]^{1/2}$$

(B-8)

The refractive indices of the liquid crystal must be known to compute the tilt from the effective birefringence. The refractive indices for MBBA have been measured, but their exact values depend on the order parameter of the liquid crystal, and thus on the difference between room temperature and the transition temperature of the liquid crystal. As the transition temperature is approached the order parameter decreases, and the birefringence decreases, due to a steady increase of the ordinary index and a decrease in the extraordinary index. The purity of MBBA affects its transition temperature. Exposure to air causes decomposition products to form due to reactions with water vapor, and the transition temperature usually drops slowly with time. Whereas pure MBBA has a transition temperature of 46°C, a sample which has been exposed to air for prolonged periods might have a transition temperature as low as 40°C. Therefore, the room-temperature values of the indices depend on the liquid crystal purity. Reference 47 gives the birefringence of MBBA as a function of $T_{NI} - T$. At room temperature the birefringence is not very sensitive to the transition temperature, since the difference in temperatures is reasonably large. The values for the indices given in Appendix C represent reasonable nominal values. Greater accuracy in the tilt measurement requires that the transition temperature be measured for each sample.

One advantage of this "wedge" technique is that fringes will be observed even if the liquid crystal layer is not unidirectionally aligned. If many randomly oriented domains of equal tilt are present, distinct fringes will be seen. Thus, the tilt angle of the liquid crystal can even be estimated when it is confined between smooth surfaces in which case it may be poorly aligned. Furthermore, if the fringes are continuous and straight as they pass from one region of the liquid crystal to another, then we can conclude that the tilt angle is identical in the two regions.



FOCAL CONDITION = $\frac{1}{d_1} + \frac{1}{d_2} = \frac{1}{f}$

$\Rightarrow d_2 = f$ as $d_1 \to \infty$

RAY FROM POINT P HAS INCIDENCE ANGLE $\theta$, SO

$h_2 = f \sin \theta$ as $d_1 \to \infty$
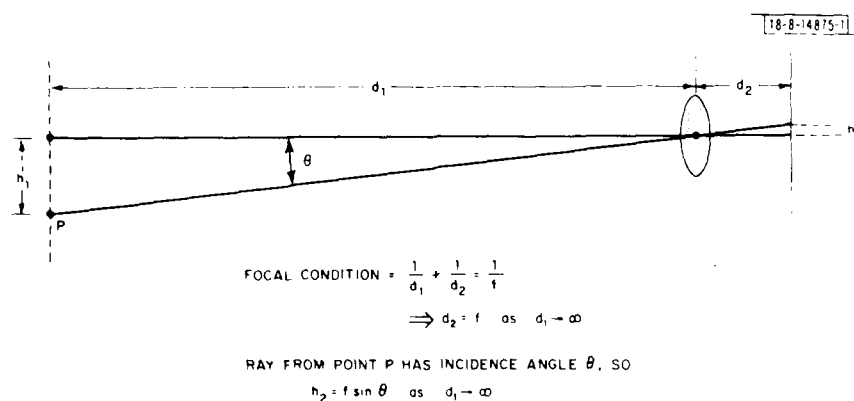
Fig. B-2. Simple ray optics showing that the conoscopic plane maps into rays of varying incidence angle.

## B.3 CONOSCOPIC TECHNIQUES USING POLARIZED LIGHT

The nematic layer can be examined in a microscope conoscopically instead of orthoscopically by using the Bertrand lens of the microscope. With the Bertrand lens in place the viewer sees a magnified image of a plane a distance f behind the objective lens, where f is the focal length of the objective. The object to be studied (nematic layer) is immediately in front of the objective.

It is easy to understand this arrangement. If the objective lens has one focal plane a distance f behind the objective, the other focal plane must be at infinity in front of the objective. The system is a telescope. Figure B-2 gives further information; it can be seen that a point at infinity will produce a point on the back focal plane. However, a point at infinity is equivalent to a plane wave with some angle of incidence, O. Thus, our conoscopic image is nothing more than a plot of the intensities of all plane waves entering the objective plotted vs angle of incidence. The point in the center of the field corresponds to a normally incident plane wave, while any ring about the center corresponds to the cone of possible rays with a given incidence angle.

This arrangement also allows the viewer to see an approximate Fourier transform of the transmissivity, $T(x, y)$, of an object in front of the objective, if the object is illuminated from behind with a monochromatic normally incident plane wave. This is shown by Fig. B-3, which is the conoscopic image of a 3.8-$\mu$m-period square-wave transmission grating, consisting of chromium lines on glass; the illumination is a well-collimated beam from a sodium lamp (5890 Å). Note that Fig. B-3 looks very similar to the two-dimensional Fourier transform of a two-dimensional square-wave intensity pattern, namely, a one-dimensional train of impulses whose intensities decay with increasing magnitude of the spatial frequency (as $(1/k) [\sin(k)]^2$. The bright center spot corresponds to zero spatial frequency.

It is quite easy to see that the conoscopic image is in fact an approximate Fourier transform as described above. First, assume that over the two-dimensional object plane (x-y) the electromagnetic field amplitude can be represented by a scalar value; simple Fourier optics, which arises from scalar diffraction theory, ignores the polarization of light. Thus, the

Fig. B-3. 3.8-$\mu$m-period grating viewed conoscopically. Illumination is at normal incidence, and is monochromatic.
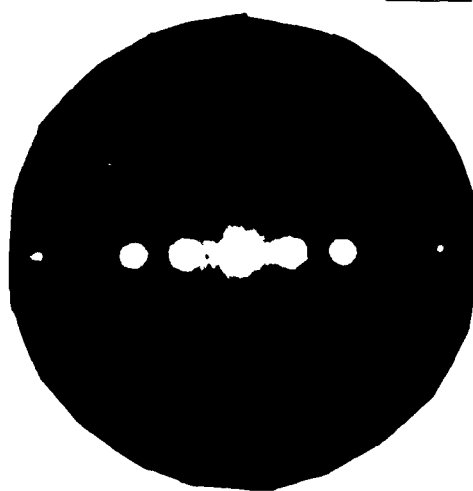
amplitude in the plane $z = 0$ is $u(x, y)$ which can obviously be represented by its Fourier transform $U(k_x, k_y)$:

$$u(x, y) = \int\!\!\int_{-\infty}^{\infty} U(k_x, k_y) \exp[ik_x x + ik_y y] \, dk_x \, dk_y \quad . \tag{B-9}$$

Now, if we consider a set of all possible plane waves, propagating or evanescent, which "propagate" in the +z direction, we find that we can represent the field throughout all space as:

$$U(x, y, z) = \int\!\!\int_{-\infty}^{\infty} a(k_x, k_y) \exp[ik_x x + ik_y y + ik_z z] \, dk_x \, dk_y \tag{B-10}$$

which reduces to Eq. (B-9) at $z = 0$, if $a(k_x, k_y) = U(k_x, k_y)$. In other words, the field amplitude at any plane in space is representable by a superposition of plane waves of identical frequency, but different propagation directions, determined by $k_x$, $k_y$, and $k_z$. Furthermore, the amplitude of a plane wave with a given propagation direction corresponds to the amplitude of a specific Fourier component. Thus, our conoscopic plane, which is a plot of the intensities of plane waves of varying angles is also a plot of the magnitude of Fourier components.

A few details should be clarified, however. We observe the Fourier transform of an object if we can produce a field amplitude which is identical to its transmissivity. This is equivalent to assuming that our normally incident plane which has a constant amplitude E in the $z = 0$ plane will pass through our object and produce a field amplitude $U(x, y) = T(x, y) E$. This is only an approximation, which tends to be valid if the apertures in the object have dimensions somewhat larger than the wavelength of the light. Furthermore, the only observable Fourier components are those which do not correspond to evanescent waves; that is, $k_z$ is real, where

$$k_z = \sqrt{k^2 - k_x^2 - k_y^2} \quad \text{and} \quad k = \frac{2\pi}{\lambda} \quad . \tag{B-11}$$

There was some doubt as to whether the specified numerical aperture of the objective lens (NA = 0.65) was indeed correct. Here, the Fourier representation proves particularly useful. Recognizing that we observe a Fourier transform of the grating, we expect components (for a grating periodic in x) with

$$k_x = m\left(\frac{2\pi}{P}\right) \tag{B-12}$$

where m is an integer, and P is the grating period.

The angles of incidence of the waves corresponding to these components are at:

$$\Theta_d = \sin^{-1}\left(\frac{k_x}{k}\right) = \sin^{-1}\left(\frac{m\lambda}{P}\right) \quad . \tag{B-13}$$

The 4th harmonic has an angle of incidence $\Theta_d = 38°$, while the 5th has $\Theta_d = 51°$. Six harmonics have propagating waves. However, the objective only accepts waves within the half angle given by:

$$\Theta_A = \sin^{-1}(NA) \quad . \tag{B-14}$$

$\theta_A = 40.5°$ for our objective, so the 5th and 6th harmonics should not be observed. In fact, Fig. B-3 reveals 9 spots corresponding to the −4th to +4th harmonics. This is direct evidence that the acceptance half angle of the objective is between $38°$ and $51°$.

The above treatment of conoscopy as a Fourier analysis process represents a slight digression, but conventional treatments of conoscopy do not touch on this highly useful topic. Conoscopic use of a microscope may prove very useful for examining periodic structures such as gratings.

When liquid crystals are examined conoscopically, a layer of uniform thickness and unidirectional optic axis orientation is placed between crossed polarizers. The sample is rotated so that the incident linearly polarized wave excites both ordinary and extraordinary waves in the liquid crystal. Furthermore, a high numerical aperture condenser is used to provide illumination with plane waves propagating in all directions through the layer.

Rays which pass through the liquid crystal layer in different directions form different angles with the optic axis, so the effective birefringence varies continuously with the angle of incidence. Since crossed polarizers are used, the birefringence information will be encoded as intensity information. The conoscopic figure represents graphically the phase lag between the ordinary and extraordinary waves as a function of incidence angle for a plane wave.

Figure B-4 illustrates conoscopic figures which were observed with a nematic liquid crystal layer. In Fig. B-4(a) the optic axis is perpendicular to the plane of the nematic layer. The pattern is concentric since the liquid crystal is symmetric about the optic axis. The center of the field is black because the ordinary and extraordinary waves are degenerate for a ray propagating along the optic axis. The black cross appears because only an ordinary or an extraordinary wave is excited for those angles of incidence.

Figure B-4(b) is the conoscopic pattern obtained when the optic axis is slightly tilted from the normal to the nematic layer. Figure B-4(c) is typical of the pattern seen for a wide range of tilts of the optic axis. Figure B-4(d) corresponds to the case where the optic axis is nearly parallel to the plane of the nematic layer. Finally, Fig. B-4(e) is the conoscopic figure when the optic axis lies in the layer.

One great feature of the conoscopic technique is that one can rapidly distinguish between perpendicular, parallel, and tilted alignments of the nematic director. The shape of the conoscopic figure tells us this without needing to know the ordinary or extraordinary refractive indices. Furthermore, for tilted alignments of the nematic director [see Figs. B-4(b) to (d)], a unique axis of symmetry exists in the pattern, and this must correspond to the direction of the nematic director projection on the plane of the layer. At least one serious disadvantage of conoscopy is that it is not very useful for poorly aligned nematic layers; if regions of equal tilt but different alignment direction are within the field of view of the objective, the conoscopic pattern may not be recognizable; in contrast, technique B.2 of this appendix may be quite effective.

Though a glance at the conoscopic pattern provides qualitative information about the tilt, quantitative information is also necessary. Specifically, the following questions arise:

(a) Most tilt angles of the director produce a pattern similar to the one in Fig. B-4(c). Over what range of tilt angles is this pattern observed? Can a tilt estimate be made by counting the number of fringes?
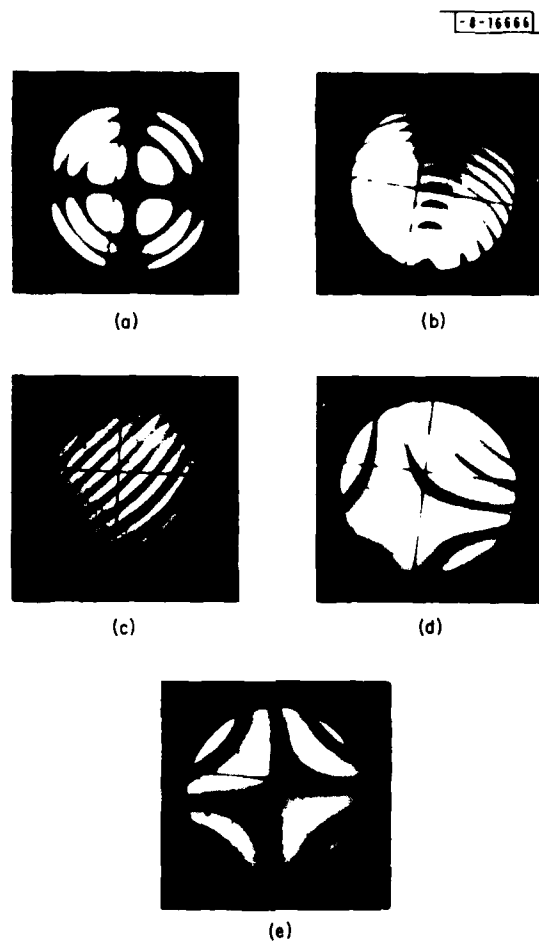
Fig. B-4. Conoscopic photos of an MBBA layer which displays many tilt angles.

(b) In Fig. B-4(e) two axes of symmetry exist and the number of fringes intersected by each axis is different. Is it possible to determine which of the two directions is the nematic director orientation by counting fringes?

It is, in fact, possible to examine the fringe patterns quantitatively. It must be stressed that tilt-angle estimation by counting conoscopic fringes does require that the refractive indices of the liquid crystal be known, and this technique is subject to the limitations discussed in Sec. B.2 of this appendix.

A computer program, CONOS3, was created to calculate the phase shift between the ordinary and extraordinary waves for rays of varying angles of incidence, and for a specified tilt of the optic axis from the normal to the nematic layer. The phase lag values are calculated only for rays whose plane of incidence is the plane formed by the normal to the layer and the optic axis; this corresponds to examining the fringe pattern along the axis of symmetry seen in Figs. B-4(b), (c), and (d). Figure B-5 is a sketch of the situation. The layer has a thickness d, the optic axis tilts at an angle $\Psi$ from the normal (note, the tilt angle is $90 - \Psi$), and the incident ray forms an angle $\Theta_i$ with the normal. For simplicity I assume that the nematic slab is bounded by air; the presence of glass substrates on both sides of the layer does not affect the computation.
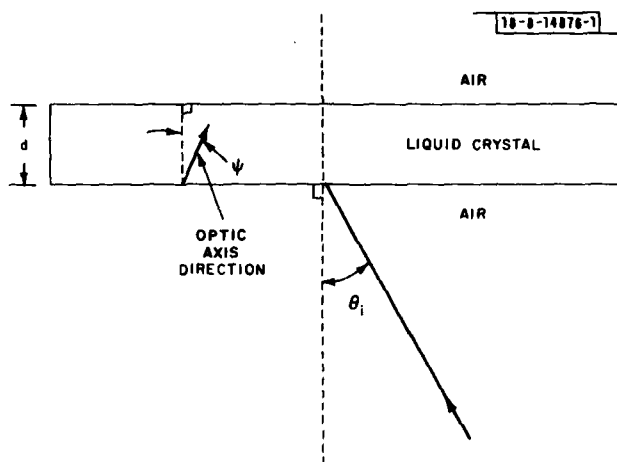


Fig. B-5. Definition of angles used in conoscopic calculations.

The incident plane wave divides into ordinary and extraordinary waves upon entering the liquid crystal, and Snell's law must be applied separately to each wave:

$$\sin\Theta_e = \frac{\sin\Theta_i}{n} \qquad (B-15)$$

$$\sin\Theta_o = \frac{\sin\Theta_i}{n_o} \qquad (B-16)$$

where $\Theta_e$ is the angle from the slab normal for the extraordinary k-vector, and $\Theta_o$ is the angle formed by the ordinary k-vector and the normal to the layer.

## TABLE B-1

| ANGLE | PHASE LAG | EXT ANGLE | ORD ANGLE | EXT INDEX |
|---|---|---|---|---|
| -42 | 3.18074 | -24.9732 | -25.5576 | 1.58488 |
| -40 | 2.91324 | -23.9687 | -24.4637 | 1.5823 |
| -38 | 2.65312 | -22.9374 | -23.3873 | 1.57973 |
| -36 | 2.40111 | -21.8806 | -22.27 | 1.57721 |
| -34 | 2.15831 | -20.7996 | -21.1332 | 1.57474 |
| -32 | 1.92556 | -19.6958 | -19.9782 | 1.57234 |
| -30 | 1.70369 | -18.5704 | -18.8065 | 1.57001 |
| -28 | 1.49302 | -17.4246 | -17.6192 | 1.56777 |
| -26 | 1.29447 | -16.2599 | -16.4177 | 1.56563 |
| -24 | 1.10865 | -15.0776 | -15.2031 | 1.56361 |
| -22 | .935745 | -13.8789 | -13.9766 | 1.5617 |
| -20 | .776529 | -12.6652 | -12.7393 | 1.55992 |
| -18 | .631237 | -11.4379 | -11.4924 | 1.55829 |
| -16 | .500441 | -10.1982 | -10.2367 | 1.5568 |
| -14 | .384331 | -8.94751 | -8.97351 | 1.55547 |
| -12 | .283003 | -7.68721 | -7.70368 | 1.5543 |
| -10 | .196886 | -6.41866 | -6.42824 | 1.5533 |
| -8 | .126171 | -5.14321 | -5.14814 | 1.55248 |
| -6 | 7.10964E-02 | -3.86224 | -3.86433 | 1.55184 |
| -4 | 3.15666E-02 | -2.57713 | -2.57775 | 1.55137 |
| -2 | 7.96318E-03 | -1.28926 | -1.28934 | 1.55109 |
| 0 | 0 | 0 | 0 | 1.551 |
| 2 | 7.96318E-03 | 1.28926 | 1.28934 | 1.55109 |
| 4 | 3.15666E-02 | 2.57713 | 2.57775 | 1.55137 |
| 6 | 7.10964E-02 | 3.86224 | 3.86433 | 1.55184 |
| 8 | .126171 | 5.14321 | 5.14814 | 1.55248 |
| 10 | .196886 | 6.41866 | 6.42824 | 1.5533 |
| 12 | .283003 | 7.68721 | 7.70368 | 1.5543 |
| 14 | .384331 | 8.94751 | 8.97351 | 1.55547 |
| 16 | .500441 | 10.1982 | 10.2367 | 1.5568 |
| 18 | .631237 | 11.4379 | 11.4924 | 1.55829 |
| 20 | .776529 | 12.6652 | 12.7393 | 1.55992 |
| 22 | .935745 | 13.8789 | 13.9766 | 1.5617 |
| 24 | 1.10865 | 15.0776 | 15.2031 | 1.56361 |
| 26 | 1.29447 | 16.2599 | 16.4177 | 1.56563 |
| 28 | 1.49302 | 17.4246 | 17.6192 | 1.56777 |
| 30 | 1.70369 | 18.5704 | 18.8065 | 1.57001 |
| 32 | 1.92556 | 19.6958 | 19.9782 | 1.57234 |
| 34 | 2.15831 | 20.7996 | 21.1332 | 1.57474 |
| 36 | 2.40111 | 21.8806 | 22.27 | 1.57721 |
| 38 | 2.65312 | 22.9374 | 23.3873 | 1.57973 |
| 40 | 2.91324 | 23.9687 | 24.4837 | 1.5823 |
| 42 | 3.18074 | 24.9732 | 25.5576 | 1.58488 |

For the extraordinary wave, n is itself a function of $\Theta_e$ as given by Eq. (B-3) where $\Theta$ is replaced by $(\Theta_e - \Psi)$. Substituting Eq. (B-3) into (B-15), we get:

$$\sin^2 \Theta_i = \frac{n_o^2 n_e^2 \sin^2 \Theta_e}{n_e^2 \cos^2 (\Theta_e - \Psi) + n_o^2 (\sin^2 \Theta_e - \Psi)} \quad . \tag{B-17}$$

After a bit of algebra, we get:

$$\Theta_e = \tan^{-1}\left(-L \pm \sqrt{L^2 - M}\right) \tag{B-18}$$

$$L = \frac{(n_e^2 - n_o^2) \sin^2 \Theta_i \cos \Psi \sin \Psi}{[\sin^2 \Theta_i (n_o^2 \cos^2 \Psi + n_e^2 \sin^2 \Psi) - n_o^2 n_e^2]} \tag{B-19}$$

$$M = \frac{\sin^2 \Theta_i (n_e^2 \cos^2 \Psi + n_o^2 \sin^2 \Psi)}{[\sin^2 \Theta_i (n_o^2 \cos^2 \Psi + n_e^2 \sin^2 \Psi) - n_o^2 n_e^2]} \quad . \tag{B-20}$$

Now, knowing the propagation direction, it is easy to get the effective extraordinary index:

$$n^2 = \frac{n_o^2 n_e^2}{n_e^2 \cos^2 (\Theta_e - \Psi) + n_o^2 \sin^2 (\Theta_e - \Psi)} \quad . \tag{B-21}$$

Now, the phase difference (in cycles) between the ordinary and extraordinary waves after passing through the layer is:

$$\varphi = \frac{1}{2\pi} (k_{ze} - k_{zo}) d$$

or

$$\varphi = \frac{d}{\lambda} (n \cos \Theta_e - n_o \cos \Theta_o) \quad . \tag{B-22}$$

The expressions above were evaluated for different values of $\Psi$ and $\Theta_i$ using CONOS3. Tables B-I to -III are for $\Psi = 0°$, $67°$, and $80°$, respectively. The acceptance half angle of the microscope objective in air is $40.5°$, so the tables represent the width of the conoscopic field. The computations are for a spacer thickness of 50 $\mu$m, $\lambda = 5890$ Å, and the values of $n_o$ and $n_e$ for MBBA (see Appendix C) were used. The column labeled PHASE LAG represents the number of cycles of phase shift [$\varphi$ of Eq. (B-22)] between the extraordinary and the ordinary waves after traversing the slab. Integer values of phase lag correspond to the centers of black conoscopic fringes.

Table B-I predicts that a 50-$\mu$m-thick layer of homeotropically oriented MBBA should produce a conoscopic pattern with 2 distinct black rings and with a 3rd ring just beyond the field edge. Figure B-6 shows the observed conoscopic figure; the agreement with the calculations is quite good.

Table B-II is calculated for $\Psi = 67°$, which corresponds to a $23°$ tilt of the optic axis from the substrate plane. Twelve black fringes are expected. Figure 6(a) (of Chap. 2) is a conoscopic figure for MBBA on fused quartz, where the tilt angle was estimated to be $23°$ using another method. Note that 12 fringes are visible. In contrast, the program would predict 11 fringes for a tilt of $20°$ or 15 fringes for a $45°$ tilt.

| | | TABLE B-II | | |
|---|---|---|---|---|
| ANGLE | PHASE LAG | EXT ANGLE | ORD ANGLE | EXT INDEX |
| -42 | 20.8677 | -22.1341 | -25.5576 | 1.77594 |
| -40 | 20.6944 | -21.2221 | -24.4837 | 1.77573 |
| -38 | 20.513 | -20.2903 | -23.3873 | 1.77538 |
| -36 | 20.3237 | -19.3398 | -22.27 | 1.77487 |
| -34 | 20.1264 | -18.3716 | -21.1332 | 1.7742 |
| -32 | 19.9211 | -17.3868 | -19.9782 | 1.77336 |
| -30 | 19.708 | -16.3863 | -18.8065 | 1.77235 |
| -28 | 19.4868 | -15.3709 | -17.6192 | 1.77115 |
| -26 | 19.258 | -14.3414 | -16.4177 | 1.76977 |
| -24 | 19.0214 | -13.2987 | -15.2031 | 1.76821 |
| -22 | 18.777 | -12.2435 | -13.9766 | 1.76645 |
| -20 | 18.5252 | -11.1765 | -12.7393 | 1.76451 |
| -18 | 18.2662 | -10.0985 | -11.4924 | 1.76238 |
| -16 | 18.0001 | -9.00995 | -10.2367 | 1.76007 |
| -14 | 17.7268 | -7.91163 | -8.97351 | 1.75757 |
| -12 | 17.4469 | -6.80414 | -7.70368 | 1.75489 |
| -10 | 17.1605 | -5.68808 | -6.42824 | 1.75203 |
| -8 | 16.8679 | -4.56403 | -5.14814 | 1.74899 |
| -6 | 16.5694 | -3.4326 | -3.86433 | 1.74579 |
| -4 | 16.2653 | -2.29439 | -2.57775 | 1.74243 |
| -2 | 15.9559 | -1.14998 | -1.28934 | 1.73892 |
| 0 | 15.6417 | 0 | 0 | 1.73520 |
| 2 | 15.3229 | 1.15494 | 1.28934 | 1.73146 |
| 4 | 15. | 2.31418 | 2.57775 | 1.72754 |
| 6 | 14.6733 | 3.47706 | 3.86433 | 1.7235 |
| 8 | 14.3434 | 4.64289 | 5.14814 | 1.71935 |
| 10 | 14.0105 | 5.81094 | 6.42824 | 1.71511 |
| 12 | 13.6754 | 6.98043 | 7.70368 | 1.71078 |
| 14 | 13.3383 | 8.15057 | 8.97351 | 1.70638 |
| 16 | 12.9998 | 9.32049 | 10.2367 | 1.70192 |
| 18 | 12.6605 | 10.4893 | 11.4924 | 1.69741 |
| 20 | 12.3209 | 11.656 | 12.7393 | 1.69297 |
| 22 | 11.9816 | 12.8196 | 13.9766 | 1.68831 |
| 24 | 11.643 | 13.9791 | 15.2031 | 1.68374 |
| 26 | 11.3058 | 15.1332 | 16.4177 | 1.67917 |
| 28 | 10.9706 | 16.2807 | 17.6192 | 1.67463 |
| 30 | 10.6379 | 17.4204 | 18.8065 | 1.67011 |
| 32 | 10.3082 | 18.5509 | 19.9782 | 1.66564 |
| 34 | 9.98259 | 19.6707 | 21.1332 | 1.66123 |
| 36 | 9.6612 | 20.7784 | 22.27 | 1.65668 |
| 38 | 9.34477 | 21.8722 | 23.3873 | 1.65261 |
| 40 | 9.03401 | 22.9505 | 24.4837 | 1.64844 |
| 42 | 8.72955 | 24.0116 | 25.5576 | 1.64437 |

| | | TABLE B-III | | |
|---|---|---|---|---|

| ANGLE | PHASE LAG | EXT ANGLE | ORD ANGLE | EXT INDEX |
|---|---|---|---|---|
| -42 | 19.7361 | -22.2973 | -25.5576 | 1.7636 |
| -40 | 19.7518 | -21.3525 | -24.4837 | 1.76539 |
| -38 | 19.7615 | -20.3898 | -23.3873 | 1.76708 |
| -36 | 19.7644 | -19.4105 | -22.27 | 1.76866 |
| -34 | 19.7603 | -18.4156 | -21.1332 | 1.77011 |
| -32 | 19.7489 | -17.4064 | -19.9782 | 1.77143 |
| -30 | 19.73 | -16.3839 | -18.8065 | 1.77259 |
| -28 | 19.7029 | -15.3491 | -17.6192 | 1.7736 |
| -26 | 19.6677 | -14.3028 | -16.4177 | 1.77445 |
| -24 | 19.6241 | -13.246 | -15.2031 | 1.77512 |
| -22 | 19.5716 | -12.1795 | -13.9766 | 1.7756 |
| -20 | 19.5104 | -11.104 | -12.7393 | 1.7759 |
| -18 | 19.4402 | -10.0202 | -11.4924 | 1.776 |
| -16 | 19.3609 | -8.92894 | -10.2367 | 1.7759 |
| -14 | 19.2727 | -7.83076 | -8.97351 | 1.77561 |
| -12 | 19.1749 | -6.72629 | -7.70368 | 1.7751 |
| -10 | 19.0679 | -5.61616 | -6.42824 | 1.77439 |
| -8 | 18.9522 | -4.50091 | -5.14814 | 1.77347 |
| -6 | 18.8271 | -3.38113 | -3.86433 | 1.77234 |
| -4 | 18.6928 | -2.25735 | -2.57775 | 1.77101 |
| -2 | 18.5497 | -1.13013 | -1.28934 | 1.76947 |
| 0 | 18.3979 | 0 | 0 | 1.76773 |
| 2 | 18.2374 | 1.13248 | 1.28934 | 1.76579 |
| 4 | 18.0684 | 2.26676 | 2.57775 | 1.76366 |
| 6 | 17.8914 | 3.40227 | 3.86433 | 1.76134 |
| 8 | 17.7064 | 4.53842 | 5.14814 | 1.75884 |
| 10 | 17.5137 | 5.67461 | 6.42824 | 1.75617 |
| 12 | 17.3139 | 6.8102 | 7.70368 | 1.75333 |
| 14 | 17.1071 | 7.94452 | 8.97351 | 1.75034 |
| 16 | 16.8938 | 9.07687 | 10.2367 | 1.7472 |
| 18 | 16.6741 | 10.2065 | 11.4924 | 1.74392 |
| 20 | 16.449 | 11.3326 | 12.7393 | 1.74052 |
| 22 | 16.2185 | 12.4543 | 13.9766 | 1.73701 |
| 24 | 15.9833 | 13.5708 | 15.2031 | 1.7334 |
| 26 | 15.744 | 14.6811 | 16.4177 | 1.7297 |
| 28 | 15.5007 | 15.7841 | 17.6192 | 1.72592 |
| 30 | 15.2545 | 16.8787 | 18.8065 | 1.72298 |
| 32 | 15.0056 | 17.9638 | 19.9782 | 1.71819 |
| 34 | 14.755 | 19.0382 | 21.1332 | 1.71427 |
| 36 | 14.503 | 20.1005 | 22.27 | 1.71033 |
| 38 | 14.2507 | 21.1493 | 23.3873 | 1.70638 |
| 40 | 13.9983 | 22.1831 | 24.4837 | 1.70244 |
| 42 | 13.7468 | 23.2003 | 25.5576 | 1.69853 |
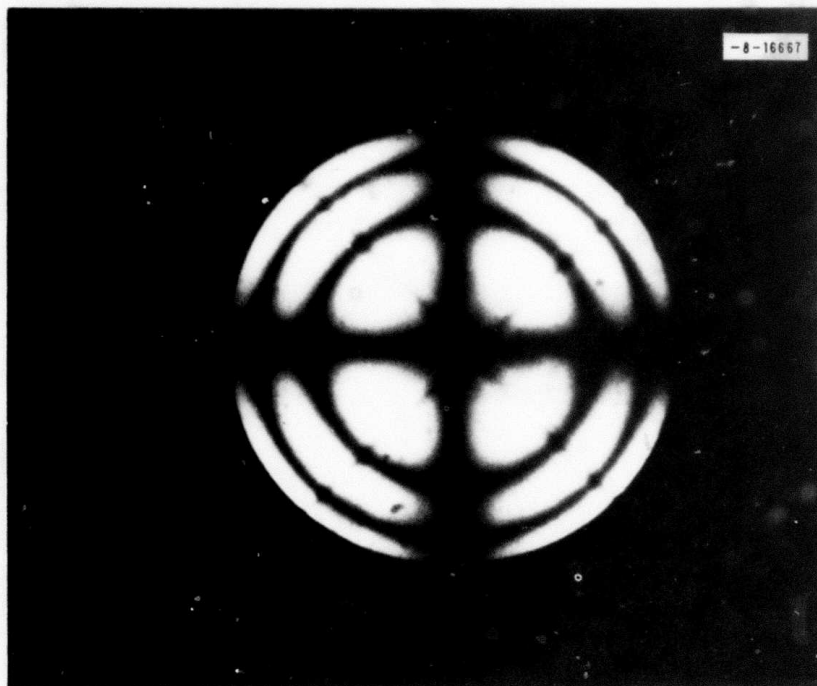
Fig. B-6.  Conoscopic photo of homeotropic MBBA layer.

For small tilts from the homeotropic orientation, the "center" of the concentric ring pattern may still be visible, as in Fig. B-4(b).  This will be the case if:

$$\Psi < \Psi_M = \sin^{-1}\left(\frac{\sin\Theta_A}{n_o}\right)$$

where $\Theta_A$ is the acceptance half angle of the objective.

For our objective used with MBBA, $\Psi_M = 25°$.  Thus, tilts within 25° of the homeotropic orientation are easily distinguished and the tilt angle can be measured without knowing the birefringence of the liquid crystal.

Figure B-4(d) shows that for small tilts from the homogeneous orientation the hyperbolic pattern persists.  Table B-III shows that for tilts greater than about 10° the hyperbolic pattern vanishes.

The remaining issue is whether, in conoscopic patterns of liquid crystals with zero tilt angle, it is possible to distinguish between the two axes of symmetry which are observed.  Hopefully, by counting fringes along each axis, the direction along the nematic director projection could be identified.  A computer program has been used to calculate the phase lag for rays of varying incidence angles with homogeneously oriented liquid crystal layers (see Tables B-IV and -V).  In the tables $\phi_{||}$ represents $\phi$ as the angle of incidence is varied in the plane which contains the optic axis; $\phi_\perp$ is calculated for angles of incidence varying perpendicular to that plane.  There are two significant features: First, the total phase shift change across the conoscopic field is greater for $\phi_{||}$ than for $\phi_\perp$, so one expects that the greater number of fringes

| | TABLE B-IV | |
|---|---|---|
| $\theta_i$ | $\phi_{\parallel}$ | $\phi_{\perp}$ |
| 0 | 19.1001 | 19.1002 |
| 1 | 19.099 | 19.1012 |
| 2 | 19.0953 | 19.1044 |
| 3 | 19.0894 | 19.1097 |
| 4 | 19.0809 | 19.1171 |
| 5 | 19.07 | 19.1266 |
| 6 | 19.0568 | 19.1382 |
| 7 | 19.0412 | 19.1519 |
| 8 | 19.0231 | 19.1678 |
| 9 | 19.0029 | 19.1856 |
| 10 | 18.9801 | 19.2056 |
| 11 | 18.955 | 19.2277 |
| 12 | 18.9278 | 19.2519 |
| 13 | 18.8983 | 19.2781 |
| 14 | 18.8665 | 19.3064 |
| 15 | 18.8324 | 19.3367 |
| 16 | 18.7962 | 19.3692 |
| 17 | 18.7577 | 19.4037 |
| 18 | 18.7172 | 19.4402 |
| 19 | 18.6747 | 19.4787 |
| 20 | 18.63 | 19.5192 |
| 21 | 18.5834 | 19.5618 |
| 22 | 18.5347 | 19.6062 |
| 23 | 18.4842 | 19.6527 |
| 24 | 18.4317 | 19.7011 |
| 25 | 18.3775 | 19.7515 |
| 26 | 18.3215 | 19.8038 |
| 27 | 18.2636 | 19.8579 |
| 28 | 18.2042 | 19.9138 |
| 29 | 18.1431 | 19.9716 |
| 30 | 18.0805 | 20.0313 |
| 31 | 18.0164 | 20.0926 |
| 32 | 17.9508 | 20.1558 |
| 33 | 17.8838 | 20.2206 |
| 34 | 17.8157 | 20.2871 |
| 35 | 17.7461 | 20.3552 |
| 36 | 17.6754 | 20.4249 |
| 37 | 17.6038 | 20.4962 |
| 38 | 17.531 | 20.5689 |
| 39 | 17.4572 | 20.6429 |
| 40 | 17.3827 | 20.7185 |
| 41 | 17.3073 | 20.7954 |

Number of fringes along optic axis projection  2
Number of fringes perpendicular to optic axis  1

| | TABLE B-V | |
|---|---|---|
| $\theta_i$ | $\phi_{\parallel}$ | $\phi_{\perp}$ |
| 0 | 19.4821 | 19.4822 |
| 1 | 19.481 | 19.4833 |
| 2 | 19.4772 | 19.4865 |
| 3 | 19.4712 | 19.4919 |
| 4 | 19.4625 | 19.4994 |
| 5 | 19.4514 | 19.5091 |
| 6 | 19.438 | 19.521 |
| 7 | 19.4221 | 19.535 |
| 8 | 19.4036 | 19.5511 |
| 9 | 19.383 | 19.5694 |
| 10 | 19.3597 | 19.5897 |
| 11 | 19.3341 | 19.6122 |
| 12 | 19.3063 | 19.6369 |
| 13 | 19.2763 | 19.6637 |
| 14 | 19.2438 | 19.6925 |
| 15 | 19.209 | 19.7235 |
| 16 | 19.1721 | 19.7566 |
| 17 | 19.1328 | 19.7918 |
| 18 | 19.0916 | 19.829 |
| 19 | 19.0481 | 19.8682 |
| 20 | 19.0026 | 19.9096 |
| 21 | 18.955 | 19.953 |
| 22 | 18.9054 | 19.9984 |
| 23 | 18.8538 | 20.0457 |
| 24 | 18.8004 | 20.0952 |
| 25 | 18.745 | 20.1465 |
| 26 | 18.6879 | 20.1998 |
| 27 | 18.6289 | 20.255 |
| 28 | 18.5682 | 20.3121 |
| 29 | 18.5059 | 20.3711 |
| 30 | 18.4421 | 20.4319 |
| 31 | 18.3767 | 20.4945 |
| 32 | 18.3098 | 20.5589 |
| 33 | 18.2415 | 20.625 |
| 34 | 18.172 | 20.6929 |
| 35 | 18.101 | 20.7623 |
| 36 | 18.0289 | 20.8334 |
| 37 | 17.9559 | 20.9061 |
| 38 | 17.8816 | 20.9803 |
| 39 | 17.8063 | 21.0558 |
| 40 | 17.7304 | 21.1329 |
| 41 | 17.6535 | 21.2113 |

Number of fringes along optic axis projection  2
Number of fringes perpendicular to optic axis  2

63

would appear along the optic axis projection. Second, the phase shift decreases along one axis while it increases along the other. This second fact means that it is actually quite difficult to figure out which axis has the greater phase shift change. This problem arises because black fringes occur only when $\phi$ is an integer; the exact value of $\phi$ at $O_i = 0$ will have a direct impact on the number of observed fringes along each axis. For Table B-IV a 50-μm-thick layer was used while for Table B-V the layer was 51 μm thick. The number of fringes seen on each axis is changed by this minor thickness variation. At most, one fringe is lost or gained, but when only one or two fringes are visible, this uncertainty is unacceptable.

To summarize, quantitative information on the tilt angle can be obtained from conoscopic figures using the procedure described above. It is difficult to distinguish between the two possible orientations of the optic axis if the liquid crystal has a zero tilt angle.

## B.4 USING DYES DISSOLVED IN A LIQUID CRYSTAL TO DETECT THE DIRECTOR ORIENTATION

Heilmeier and Zanoni[48,49] have shown that certain dye molecules will align with the director when they are dissolved in nematic liquid crystals. For instance, rod-shaped dye molecules may have a tendency to align with the roughly rod-shaped liquid crystal molecules. Furthermore, elongated organic dye molecules typically have different absorption coefficients parallel and perpendicular to their molecular axes.

The dye DODCI* aligns with its long axis parallel to the nematic director; it also absorbs light at the red end of the spectrum if the incident light is polarized along the molecular axis. If an aligned nematic layer doped with DODCI is observed by passing a linearly polarized beam of white light through it, then the liquid crystal will look blue when the incident polarization is along the director and clear when the polarization is perpendicular to the director.

This method is useful for identifying the direction of the nematic director unambiguously in cases when the tilt angle of the liquid crystal is zero.

## B.5 QUALITATIVE TILT-ANGLE INFORMATION FROM SCHLIEREN TEXTURES

The examination of Schlieren textures permits rapid discrimination between parallel and tilted director alignment. Schlieren textures are discussed in Chaps. 2 and 3. Schlieren textures often contain disclinations of strength 1/2, where the nematic director projection undergoes a 180° rotation. In nematics with nonzero tilt, a fine line will be seen attaching to these disclinations. This line represents a boundary between regions of reverse tilt. In Fig. 5(a) such lines can be seen to originate from disclinations with two black brushes (which have strength = 1/2).

---

* DODCI, Eastman Kodak 14351, called 3, 3'-diethyloxadicarbocyanine iodide; actually, 3-ethyl-2-[5-(3-ethyl-2-benzoxazolinylidene)-1, 3-pentadienyl] benzoxazolium iodide.

# APPENDIX C

## PHYSICAL PROPERTIES OF LIQUID CRYSTALS

### MBBA

Refractive index values are from Introduction to Liquid Crystals, p. 352 (see Ref. 29).

| Room Temperature | | |
|---|---|---|
| Refractive Indices | | |
| Wavelength | $n_o$ | $n_e$ |
| 5145 Å | 1.5616 | 1.8062 |
| 6328 Å | 1.5443 | 1.7582 |
| Interpolated | 1.551 | 1.776 |
| 5890 Å value | | |

The interpolated value was used for all tilt-angle calculations.

MBBA changes from crystalline to nematic at 19°C.

The nematic-isotropic transition temperature is typically at 41° to 46°C.

### M24

This liquid crystal is manufactured by BDH Chemicals, Ltd., Poole Dorset, England. It changes from crystalline to smectic A at 54.5°C. The smectic to nematic transition is at 66.5°C. The nematic-isotropic transition temperature is 78.3°C.

### Heptyl/Butyl Mixture

This consists of a 2:1 molar ratio of p-cyanophenyl p-heptylbenzoate (Eastman 14047) and p-cyanophenyl p-butylbenzoate (Eastman 14044). This liquid crystal has a large positive dielectric anisotropy, and is useful in twisted nematic display devices.[34]

# REFERENCES

1. F. J. Kahn, G. N. Taylor, and H. Schonhorn, "Surface-Produced Alignment of Liquid Crystals," Proc. IEEE 61, 823 (1973).

2. P. G. de Gennes, The Physics of Liquid Crystals (Clarendon Press, Oxford, 1974), p. 71.

3. Op. cit., p. 63.

4. H. Zocher and K. Coper, "On Rendering Surfaces Anisotropic," translation of Z. Phys. Chem. 132, 295 (1928). Translation is in The Glass Industry 30, 272 (1949).

5. D. C. Flanders, "Orientation of Crystalline Overlayers on Amorphous Substrates by Artificially Produced Surface Relief Structures," PhD. Thesis, Massachusetts Institute of Technology, January 1978; also, Technical Report 533, Lincoln Laboratory, M.I.T. (5 December 1978), DDC AD-071168.

6. F. J. Kahn, "Orientation of Liquid Crystals by Surface Coupling Agents," Appl. Phys. Lett. 22, 386 (1973).

7. J. E. Proust and L. Ter-Minassian-Saraga, "Orientation of a Nematic Liquid Crystal by Suitable Boundary Surfaces," Solid State Commun. 11, 1227 (1972).

8. E. Perez, J. E. Proust, and L. Ter-Minassian-Saraga, "Interfacial Origin of Liquid Crystal Anchorage," Mol. Cryst. Liq. Cryst. 42, 167 (1977).

9. L. T. Creagh and A. R. Kmetz, "Mechanism of Surface Alignment in Nematic Liquid Crystals," Mol. Cryst. Liq. Cryst. 24, 59 (1973).

10. D. W. Berreman, "Solid Surface Shape and the Alignment of an Adjacent Nematic Liquid Crystal," Phys. Rev. Lett. 28, 1683 (1972).

11. _____, "Alignment of Liquid Crystals by Grooved Surfaces," Mol. Cryst. Liq. Cryst. 23, 215 (1973).

12. U. Wolff, W. Greubel, and H. Kruger, "The Homogeneous Alignment of Liquid Crystal Layers," Mol. Cryst. Liq. Cryst. 23, 187 (1973).

13. J. L. Janning, "Thin Film Surface Orientation for Liquid Crystals," Appl. Phys. Lett. 21, 173 (1972).

14. L. I. Maissel and R. Glang, Handbook of Thin Film Technology (McGraw-Hill, New York, 1970), pp. 15-9 and 15-10.

15. E. Guyon, P. Pieranski, and M. Boix, "On Different Boundary Conditions of Nematic Films Deposited on Obliquely Evaporated Plates," Lett. Appl. Eng. Sci. 1, 19 (1973).

16. W. Urbach, M. Boix, and E. Guyon, "Alignment of Nematics and Smectics on Evaporated Films," Appl. Phys. Lett. 25, 479 (1974).

17. D. Meyerhofer, "New Technique of Aligning Liquid Crystals on Surfaces," Appl. Phys. Lett. 29, 691 (1976).

18. M. R. Johnson and P. A. Penz, "Low-Tilt-Angle Nematic Alignment Compatible with Frit Sealing," IEEE Trans. Electron Devices ED-24, 805 (1977).

19. L. A. Goodman, J. T. McGinn, C. H. Anderson, and F. DiGeronimo, "Topography of Obliquely Evaporated Silicon Oxide Films and Its Effect on Liquid Crystal Orientation," IEEE Trans. Electron Devices ED-24, 795 (1977).

20. G. D. Dixon, T. P. Brody, and W. A. Hester, "Alignment Mechanism in Twisted Nematic Layers," Appl. Phys. Lett. 24, 47 (1974).

21. M. J. Little, H. L. Garvin, and L. J. Miller, "A New Method for Inducing Homogeneous Alignment of Nematic Liquid Crystals," preprint only, Hughes Research Laboratories, Malibu, California.

22. L. J. Miller, J. Grinberg, G. D. Myer, D. S. Smythe, and W. H. Smith, "A New Method for Inducing Homeotropic and Tilted Alignments of Nematic Liquid Crystals on Silica Surfaces," preprint only, Hughes Research Laboratories, Malibu, California.

23. D. C. Flanders, D. C. Shaver, and H. I. Smith, "Alignment of Liquid Crystals Using Submicrometer Periodicity Gratings," Appl. Phys. Lett. 32, 597 (1978).

24. J. Nehring and A. Saupe, "On the Schlieren Texture in Nematic and Smectic Liquid Crystals," Chem. Soc. J. Faraday Trans. II 68, 1 (1972).

25. A. Saupe, "Disclinations and Properties of the Directorfield in Nematic and Cholesteric Liquid Crystals," Mol. Cryst. Liq. Cryst. 21, 211 (1973).

26. H. Sackmann and D. Demus, "The Problems of Polymorphism in Liquid Crystals," Mol. Cryst. Liq. Cryst. 21, 239 (1973).

27. P. G. de Gennes, see Ref. 2, p. 125 ff.

28. I. Haller, "Alignment and Wetting Properties of Nematic Liquids," Appl. Phys. Lett. 24, 349 (1974).

29. L. A. Goodman, "Liquid Crystal Displays — Packaging and Surface Treatments," in Introduction to Liquid Crystals, E. B. Priestley, P. J. Wojtowicz, and P. Sheng, Eds. (Plenum Press, New York, 1975), p. 231.

30. J. R. Vig, "UV/Ozone Cleaning of Surfaces," IEEE Trans. Parts, Hybrids, and Packaging PHP-12, 365 (1976).

31. M. A. Bouchiat and D. Langevin-Cruchon, "Molecular Order at the Free Surface of a Nematic Liquid Crystal from Light Reflectivity Measurements," Phys. Lett. 34A, 331 (1971).

32. D. Langevin and M. A. Bouchiat, "Molecular Order and Surface Tension for the Nematic-Isotropic Interface of MBBA, Deduced from Light Reflectivity and Light Scattering Measurements," Mol. Cryst. Liq. Cryst. 22, 317 (1973).

33. R. B. Meyer, "Point Disclinations at a Nematic-Isotropic Liquid Interface," Mol. Cryst. Liq. Cryst. 16, 355 (1972).

34. A. Boller, H. Scherrer, and M. Schadt, "Low Electrooptic Threshold in New Liquid Crystals," Proc. IEEE 60, 1002 (1972).

35. P. J. Wojtowicz, "Introduction to the Molecular Theory of Nematic Liquid Crystals," in Introduction to Liquid Crystals, E. B. Priestley, P. J. Wojtowicz, and P. Sheng, Eds. (Plenum Press, New York, 1975).

36. M. Schadt and W. Helfrich, "Voltage Dependent Optical Activity of a Twisted Nematic Liquid Crystal," Appl. Phys. Lett. 18, 127 (1971).

37. L. A. Goodman, "Liquid Crystal Displays — Electro-optic Effects and Addressing Techniques," in Introduction to Liquid Crystals (see Ref. 35).

38. G. R. Bird and M. Parrish, Jr., "The Wire Grid as a Near Infrared Polarizer," J. Opt. Soc. Am. 50, 886 (1960).

39. T. Larsen, "A Survey of the Theory of Wire Grids," IRE Trans. Microwave Theory Tech. MTT-10, 191 (1962).

40. Y. Poggi, R. Aleonard, and J. Robert, "Transition of an Oriented Nematic Liquid Crystal to a Glass with a Nematic Order - Determination of the Order Parameter," Phys. Lett. 54A, 393 (1975).

41. J. E. Lydon and J. O. Kessler, "Phase Transitions Observed on Warming Fast-Quenched MBBA," J. Phys. (Paris), Supplement C1, 36, C1-153 (1975).

42. J. O. Kessler and E. P. Raynes, "Glassy Liquid Crystals: Observation of a Quenched Twisted Nematic," Phys. Lett. 50A, 335 (1974).

43. D. C. Flanders, H. I. Smith, H. W. Lehmann, R. Widmer, and D. C. Shaver, "Surface Relief Structures with Linewidths Below 2000 Å," Appl. Phys. Lett. 32, 112 (1978).

44. H. W. Lehmann and R. Widmer, "Fabrication of Deep Square Wave Structures with Micron Dimensions by Reactive Sputter Etching," Appl. Phys. Lett. 32, 16? (1978).

45. H. I. Smith, N. Efremow, and P. L. Kelley, "Photolithographic Contact Printing of 4000 A Linewidth Patterns," J. Electrochem. Soc. 121, 1503 (1974).

46. E. E. Wahlstrom, Optical Crystallography (Wiley, New York, 1960), p. 142.

47. I. Haller, H. A. Huggins, and M. J. Freiser, "On the Measurement of Indices of Refraction of Nematic Liquids," Mol. Cryst. Liq. Cryst. 16, 53 (1972).

48. G. H. Heilmeier and L. A. Zanoni, "Guest-Host Interactions in Nematic Liquid Crystals. A New Electro-optic Effect," Appl. Phys. Lett. 13, 91 (1968).

49. _____, "Guest-Host Interactions in Nematic Liquid Crystals," Mol. Cryst. Liq. Cryst. 8, 293 (1969).

SECURITY CLASSIFICATION OF THIS PAGE *(When Data Entered)*

| REPORT DOCUMENTATION PAGE | | READ INSTRUCTIONS BEFORE COMPLETING FORM |
|---|---|---|
| 1. REPORT NUMBER<br>ESD-TR-79-267 | 2. GOVT ACCESSION NO.<br>AD-A086816 | 3. RECIPIENT'S CATALOG NUMBER |
| 4. TITLE *(and Subtitle)*<br><br>Alignment of Liquid Crystals by Surface Gratings | | 5. TYPE OF REPORT & PERIOD COVERED<br><br>Technical Report |
| | | 6. PERFORMING ORG. REPORT NUMBER<br>Technical Report 538 |
| 7. AUTHOR(s)<br><br>David C. Shaver | | 8. CONTRACT OR GRANT NUMBER(s)<br><br>F19628-80-C-0002 |
| 9. PERFORMING ORGANIZATION NAME AND ADDRESS<br><br>Lincoln Laboratory, M.I.T.<br>P.O. Box 73<br>Lexington, MA 02173 | | 10. PROGRAM ELEMENT, PROJECT, TASK AREA & WORK UNIT NUMBERS<br>ARPA Order 3336<br>Program Element No. 61101E<br>Project No. 8D1000 |
| 11. CONTROLLING OFFICE NAME AND ADDRESS<br><br>Defense Advanced Research Projects Agency<br>1400 Wilson Boulevard<br>Arlington, VA 22209 | | 12. REPORT DATE<br>31 October 1979 |
| | | 13. NUMBER OF PAGES<br>76 |
| 14. MONITORING AGENCY NAME & ADDRESS *(if different from Controlling Office)*<br><br>Electronic Systems Division<br>Hanscom AFB<br>Bedford, MA 01731 | | 15. SECURITY CLASS. *(of this report)*<br><br>Unclassified |
| | | 15a. DECLASSIFICATION DOWNGRADING SCHEDULE |

16. DISTRIBUTION STATEMENT *(of this Report)*

Approved for public release; distribution unlimited.

17. DISTRIBUTION STATEMENT *(of the abstract entered in Block 20, if different from Report)*

18. SUPPLEMENTARY NOTES

None

19. KEY WORDS *(Continue on reverse side if necessary and identify by block number)*

liquid crystals          grating polarizers          surface gratings

20. ABSTRACT *(Continue on reverse side if necessary and identify by block number)*

Square-wave grating structures with periodicities ranging from 3200Å to 12 μm were etched into fused quartz substrates, and the effect of such gratings on liquid crystal alignment was studied. Gratings with periodicities below 4 μm appear to be required to align typical room-temperature nematic liquid crystals. At larger periodicities a pronounced defect texture forms, due to an adsorbed liquid crystal layer which forms during nucleation of the nematic phase.

Surface gratings were also formed by patterning a "monolayer" of DMOAP. Such patterned organic monolayers, which have no appreciable surface relief, are effective at aligning liquid crystals. This represents a new approach to liquid crystal alignment.

High-quality alignment of the smectic A phase of M24 was induced by a 3200-Å-period square-wave surface-relief grating.

A novel twisted-nematic liquid crystal display which uses metal gratings for polarization of light as well as for liquid crystal alignment was fabricated.

DD FORM 1473  EDITION OF 1 NOV 65 IS OBSOLETE
1 JAN 73

✢ U.S. GOVERNMENT PRINTING OFFICE: 1980 - 600-039/15